4. Ocean Modelling and Prediction

Matthew H. England and Peter R. Oke

4.1 Introduction

The ocean plays a vital role in our environment. As such, an ability to model and predict its circulation can be of enormous value. Modelling and prediction of ocean currents in coastal regions is important for many reasons, including influences on recreation, navigation, algal bloom formation, effluent dispersion, search and rescue operations, and oil spills. Ocean currents near the coast also affect beach conditions that impact upon the near-shore zone. Severe wave climates and storm surges can cause enormous destruction of the built environment. At larger scales, vast ocean currents carry heat around the globe, affecting climate and weather patterns such as those associated with the El-Niño event and the North Atlantic Oscillation. The oceans also have a vast capacity to absorb and redistribute gases such as carbon dioxide. They will therefore play a crucial role in determining our future climate.

To understand and predict the way the ocean affects our environment, a number of ocean models have been developed during the past half century. Some are computationally simple and predict a limited number of oceanic variables, such as tidal models or a wave climate model. Others, such as primitive equation ocean general circulation models (OGCMs), are computationally expensive and solve several equations in order to predict three-dimensional ocean currents and temperature-salinity ($T-S$). In this chapter we describe the state-of-the-art in ocean modelling.

4.1.1 What Is an Ocean Model?

The World's oceans can be viewed as a turbulent stratified fluid on a rotating sphere with a multiply-connected domain and an uneven bottom bathymetry. More simply, the rotating earth has an ocean system divided by land masses and with varying water density and ocean depth. The external forcing of the ocean occurs through the mechanical forcing of the winds, the so-called "thermohaline" forcing via heat and freshwater fluxes across the air-sea interface, and through planetary forces manifest in tides. An ocean model is simply a computational solution to this problem: using physical conservation laws for mass, momentum, heat and so on, and some estimation of the forcing fields, the computer model predicts ocean currents and other properties such as temperature, salinity, and optionally chemical tracers or biological parameters.

4.1.2 Mean Large-scale Ocean Circulation

The global scale ocean circulation can be viewed in a number of ways. In the horizontal plane, mean circulation is dominated in the upper ocean by wind-driven flow. Figure 4.1 shows surface mean wind stress over the oceans, and the upper ocean circulation pattern. Large-scale gyres dominate at mid-latitudes, with intensified western boundary currents (WBCs) due to the Earth's rotation, carrying tropical heat poleward. At the tropics, easterly trade winds and the doldrums drive a tropical current/counter current system (for more details see Tomczak and Godfrey, 1994). At higher latitudes thermohaline circulation is manifest in the surface flow; for example, the North Atlantic Current extends into the Greenland/Norwegian Sea to feed North Atlantic Deep Water formation. In the Southern Ocean, a latitude band free of continental land masses permits the eastward flowing Antarctic Circumpolar Current (ACC) to circle the globe.

In the meridional plane a completely different view of the ocean circulation is obtained (Fig. 4.2). Water masses of different density classes ventilate the interior of the ocean in a complex manner. Around Antarctica dense bottom water is formed over the continental shelf by salt rejection during sea-ice formation and wintertime cooling. Further north, Circumpolar Deep Water (CDW) is upwelled under the subpolar westerlies, flowing either northward to form intermediate and mode waters (after the addition of freshwater via precipitation or sea-ice melt), or southward towards the Antarctic continent. In the Northern Hemisphere, a saltier North Atlantic accommodates deep water production whereas the North Pacific remains too fresh to see deep water convection. The water masses formed in the World Ocean subsequently recirculate and are either "consumed" by diapycnal mixing or when they resurface in the upper mixed layer. In both cases, $T-S$ properties are altered or reset and the water-mass is converted.

4.1.3 Oceanic Variability

The dominant picture of ocean circulation at the large-scale was one of steady flow until drifting buoy technologies in the 1960s revealed variability of flow patterns at rather small spatial scales. Near-shore variability was long known to exist and was thought to be controlled by fluctuations in tidal flows and local winds. At the large-scale, oceanic variability is evident in phenomena such as El-Niño and the Antarctic Circumpolar Wave; as well as in western

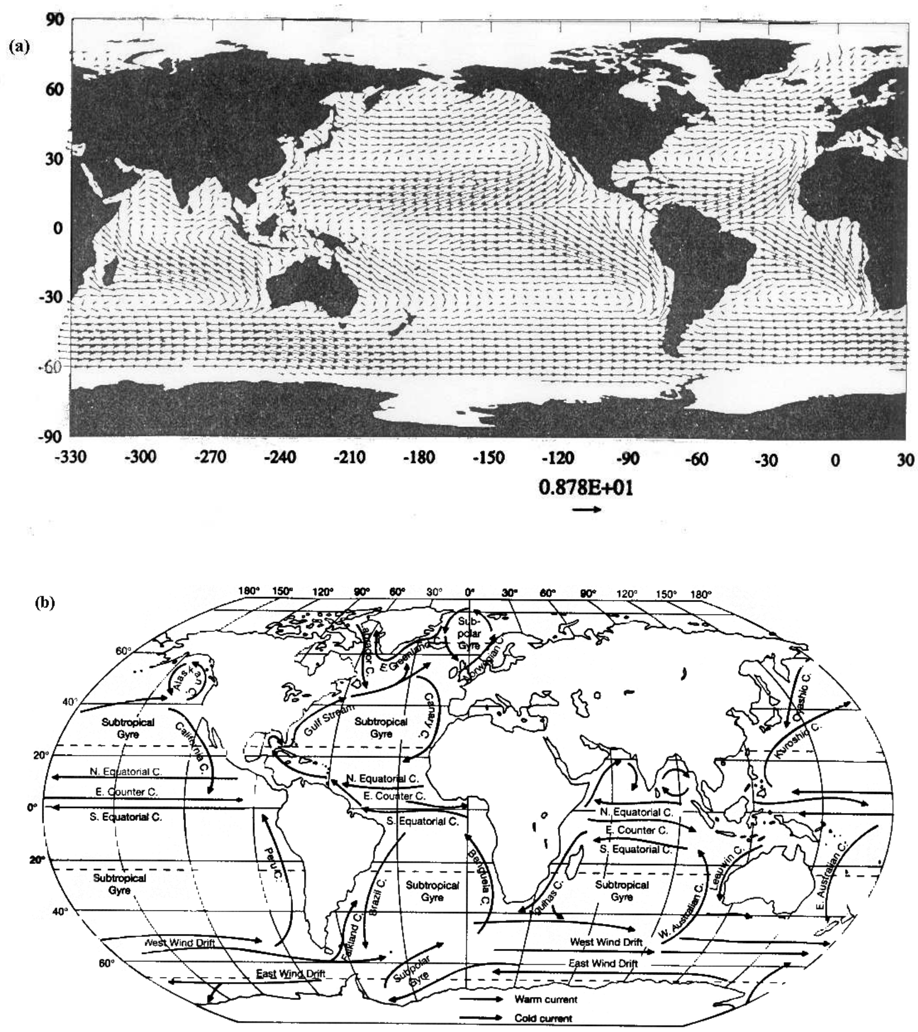

Fig. 4.1. (**a**) Surface mean wind stress over the oceans (from Barnier, 1998); and (**b**) Schematic of upper ocean circulation patterns (from Thurman, 1991).

boundary current flow pathways. In addition, oceanic eddies of size 30–100 km are seen near intense surface currents (e.g. the ACC and WBCs) and near the Equator, and play a key role in transporting climate properties around the globe. Figure 4.3 shows the kinetic energy spectrum estimated for the ocean and atmosphere as a function of horizontal wavenumber, revealing substantial oceanic energy at the length scale of these mesoscale eddies. Unfortunately, most present day coupled climate models do not resolve these scales of mo-

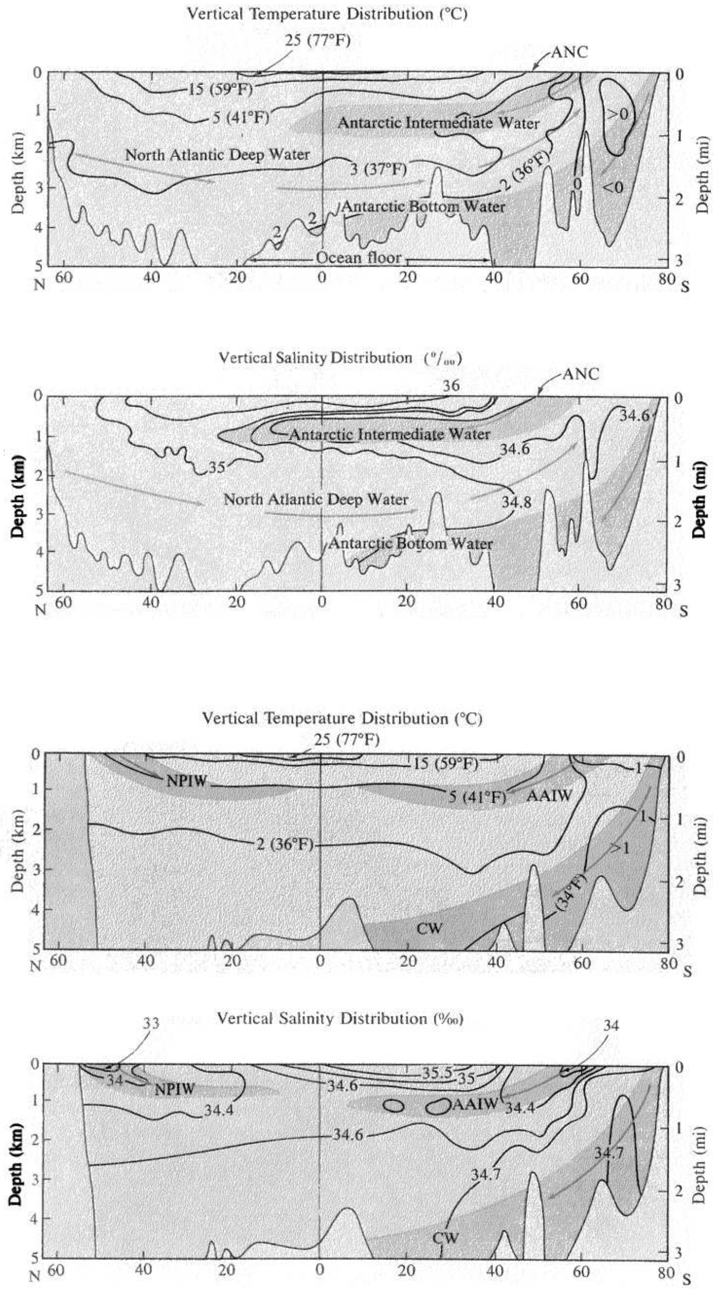

Fig. 4.2. Meridional latitude-depth ocean circulation schematics for the Pacific and Atlantic Oceans (from Thurman, 1991). AAIW refers to Antarctic Intermediate Water, NPIW to North Pacific Intermediate Water, and ANC to the Antarctic Convergence.

tion as computational requirements are too high at sub-eddy scale resolutions. These models adopt large-scale eddy parameterisations to permit reasonable model integration times. Coastal or regional models, as well as global simulations over shorter integration periods, can resolve mesoscale eddy variability (see, e.g., Semtner and Chervin, 1992; Webb et al., 1998).

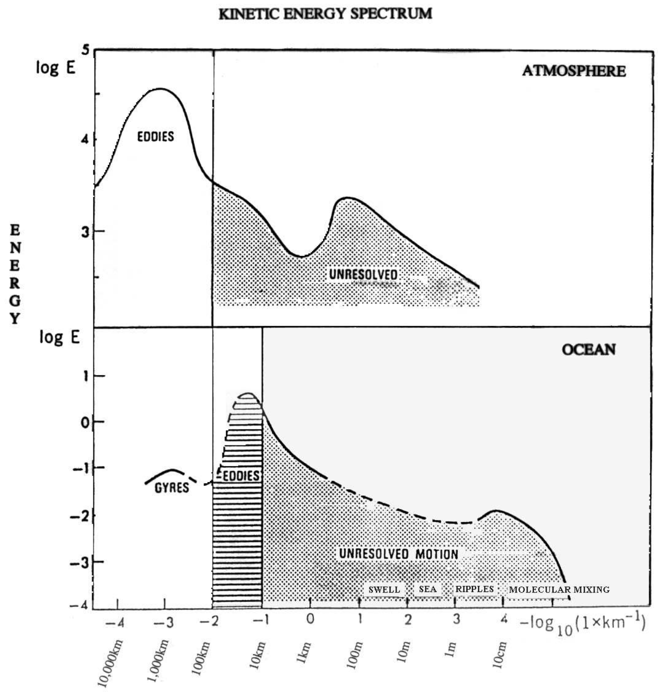

Fig. 4.3. Kinetic energy spectrum estimated for the ocean and atmosphere as a function of horizontal wavenumber (after Woods, 1985).

4.1.4 The Oceans, Climate, and Forcing

The oceans play a vital role in the global climate system via their capacity to absorb heat in certain locations, transport this heat vast distances, then release some of it back to the atmosphere at a later time. This is depicted in Fig. 4.4 which shows the global mean transport of heat by the oceans. This pattern of heat transport reflects the effects of western boundary currents carrying warm water poleward, as well as the net flux of heat towards deep water formation sites, particularly NADW. The ocean exhibits variability on a range of space-time scales, and some of this variability is at a large enough spatial scale to affect global weather systems. For example, the El-Niño/Southern Oscillation (ENSO) involves a massive redistribution of heat in the tropical Pacific Ocean via anomalous surface circulation patterns (see Philander, 1990 for details). In the Southern Ocean, the Antarctic Circumpolar Wave (ACW) advects heat anomalies around the globe, affecting wind patterns, pressure systems and sea-ice extent. Ocean modelling for climate studies has arisen from the need to understand and predict the way ocean circulation can vary and affect weather/climate. Given that the ocean circulation is determined by both wind and thermohaline factors, ocean climate models generally include both these forces whilst neglecting high frequency waves such as tides and swell.

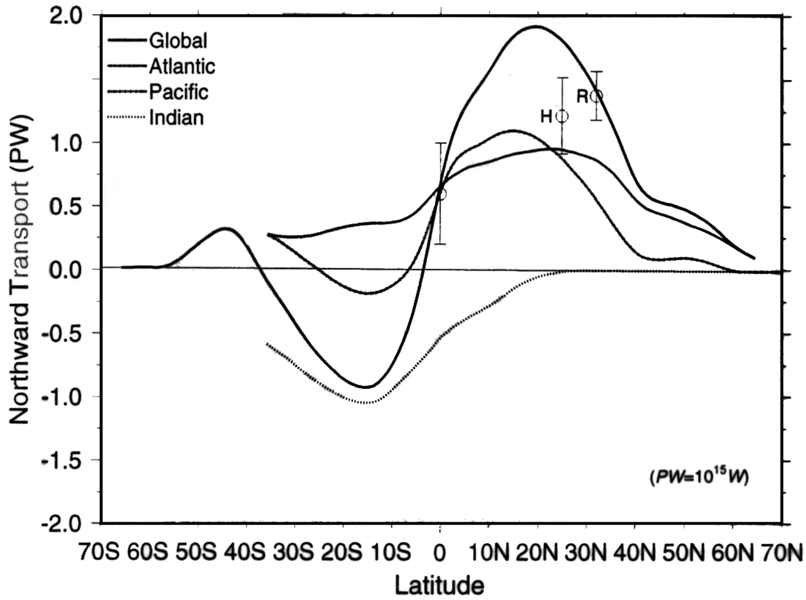

Fig. 4.4. Global mean transport of heat by the oceans (from Mathieu, 1999; using observations of da Silva et al., 1994).

Coastal ocean currents are affected by a number of different factors including winds, surface heating, buoyancy effects, tides, deep ocean forcing (e.g. WBCs) and coastal trapped waves (CTWs). The time scales on which many of these factors vary are from weather-band (3–7 days) to seasonal scales. Winds tend to be the most dominant force, locally affecting ocean currents, temperature and salinity (through upwelling/downwelling) and sea-level. Buoyancy effects often become important in response to wind-driven events (through geostrophic adjustment), in the presence of river outflows, or in regions where a significant amount of heat is gained or lost at the ocean surface. In many coastal regions tides are important [e.g., the North West Australian shelf (Holloway, 1984)] and in others deep ocean forcing is predominant [e.g., off eastern Australia (Oke and Middleton, 2000)]. Modelling the coastal ocean is therefore a challenging task, and consideration of what factors are most important for any particular region is necessary in order to adequately represent the true variability of the coastal ocean. At smaller scales, such as flows in harbours or bays, circulation patterns are often dominated by tidal flows, so their modelling can be simplified somewhat.

4.2 A Brief History of Ocean Modelling

A number of simple analytic and linear vorticity models of the basin-scale ocean circulation were developed prior to the proliferation of computing machines, including the so-called Sverdrup model of wind-driven flow (Welander, 1959), the Stommel-Arons model of abyssal circulation (Stommel and Arons, 1960), and Wyrtki's (1961) simple model of thermal overturning circulation. For a review of these early analytic modelling efforts the reader is referred to Weaver and Hughes (1992). Similarly, analytic models of wind-driven coastal jets (Allen, 1973), continental shelf waves (Allen, 1980) and stratified flows over sloping topography (Chapman and Lentz, 1997) have given modellers great insight into the dynamics of coastal ocean flows.

The first real progress towards a primitive euqation ocean circulation model came with the work of Kirk Bryan and Michael Cox in the 1960s (Bryan and Cox, 1967, 1968), in pioneering work towards a coupled climate model. They developed a model of ocean circulation carrying variable $T-S$ (and therefore density) based upon the conservation equations for mass, momentum, heat and moisture, and the equation of state. It is not surprising this work was completed at an institution where atmospheric modelling was already well-established (the GFDL), as the ocean and atmosphere have a number of similarities, and their modelling requires many analogous techniques. Bryan-Cox assumed the ocean had negligible variations in sea-level (i.e. the "rigid-lid" approximation), so that high-frequency gravity waves are ignored in the model formulation, and the depth-averaged component of velocity (the "barotropic" mode) is solved using an iterative technique. Their model was configured in a variety of ways: a 2-D model, a 3-D basin model, and a full World Ocean model (Cox, 1975).

The computational requirements of this early model were relatively high, enabling only short integrations from initial conditions, and therefore solutions that were not in thermodynamic equilibrium with the model forcing. Nevertheless, Bryan-Cox achieved global simulations with realistic continental outlines, rough bottom bathymetry, prognostic equations for $T-S$, an elimation of high frequency modes, and approximate closure schemes for the effects of mixing, friction, and eddies. Their work can be seen as the genesis of modern-day ocean modelling.

Since the early efforts of Bryan and Cox, a great number of ocean model developments have occurred (for an outstanding review, see Griffies et al., 2001). These include the exploration of different grid systems. The GFDL model operates on a Cartesian grid with geopotential (i.e., horizontal) layers in the vertical. Models have now been developed with terrain-following (Haidvogel et al., 1991) and density-layer coordinates (Bleck and Boudra, 1986). In the horizontal plane, models have been developed with curvilinear coordinates to follow a local coastline (Blumberg and Mellor, 1987).

In addition to different grid systems, a great variety of model options have been developed. In models that do not explicitly resolve mesoscale eddies, their effects can be parameterised in a number of ways (e.g., Cox, 1987; Redi, 1982; Gent and McWilliams, 1990; Gent et al., 1995; Griffies et al., 1997). Free surface formulations were also developed to enable direct prediction of the height and pressure of the ocean surface (e.g., Killworth et al., 1991; Dukowicz and Smith, 1994). This enabled direct comparison with satellite-derived data products as well as eliminating the need to solve the barotropic streamfunction iteratively (which becomes costly in higher resolution model domains and when multiple islands are involved).

Ocean model development has now proliferated due to improved numerical techniques, better global ocean data sets, diversity of model applications, and perhaps most dramatically, faster computers with ever increasing processing capacity.

4.3 Anatomy of Ocean Models

4.3.1 Governing Physics and Equations

Ocean models are capable of predicting a number of variables, normally the three components of velocity (u, v, w), temperature (T)–salinity (S) and therefore density (ρ). They also usually predict either the depth-integrated transport streamfunction or the sealevel pressure. These "predicted" variables are known as the model "prognostic" variables. To build an ocean model requires a number of governing equations in order to solve for the prognostic variables. To have a well-determined system requires the number of equations to be the same as the number of prognostic variables. For large-scale or regional coastal ocean models the governing equations are derived from the conservation laws of mass, heat and salt as well as the Navier-Stokes equations for flow of fluid on a rotating earth. Typically modellers reduce the latter to the so-called "primitive equations" by adopting the *Boussinesq* and *hydrostatic* approximations, meaning respectively that density variations do not affect the momentum balance except via the vertical buoyancy force (that is, density variations ρ are much less than the total density ρ_0), and that the buoyancy force is balanced solely by the vertical pressure gradient (therefore it is assumed that vertical velocities are small compared to horizontal velocities). These assumptions are valid in almost all oceanic circulation regimes; a notable exception being oceanic convection of unstably stratified waters (discussed later) wherein nonhydrostatic flow occurs.

The primitive equations operating in ocean models are depicted in the schematic diagram of Fig. 4.5, which shows how the equations are interrelated as well as what surface forcing is required (see also Sect. 4.3.4).

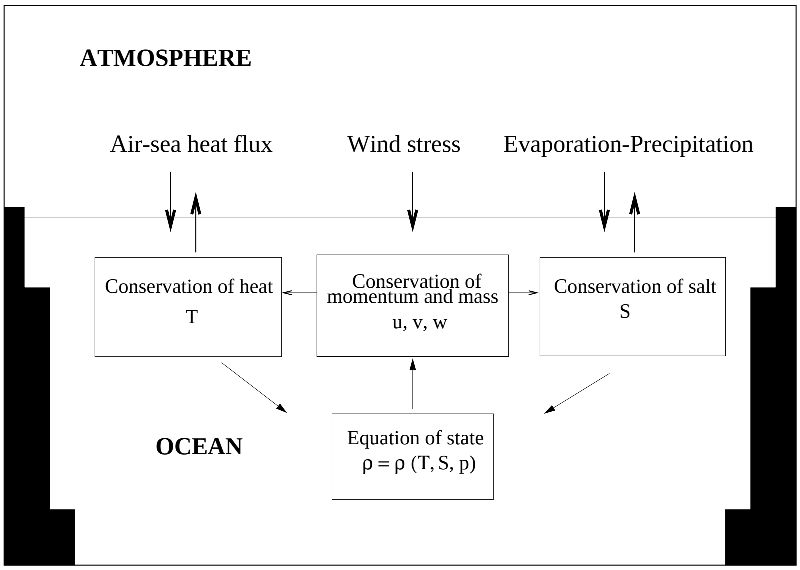

Fig. 4.5. Schematic diagram showing the conservation laws, prognostic variables, and air-sea property fluxes used in ocean models.

The model equations can be written in Cartesian coordinates as follows.

Horizontal momentum equations:

$$\frac{\mathrm{d}u}{\mathrm{d}t} - fv = \frac{\partial u}{\partial t} + u\frac{\partial u}{\partial x} + v\frac{\partial u}{\partial y} + w\frac{\partial u}{\partial z} - fv = -\frac{1}{\rho_0}\frac{\partial p}{\partial x} + F_u + D_u \quad (4.1)$$

$$\frac{\mathrm{d}v}{\mathrm{d}t} + fu = \frac{\partial v}{\partial t} + u\frac{\partial v}{\partial x} + v\frac{\partial v}{\partial y} + w\frac{\partial v}{\partial z} + fu = -\frac{1}{\rho_0}\frac{\partial p}{\partial y} + F_v + D_v \quad (4.2)$$

Hydrostatic approximation:

$$\rho g = -\frac{\partial p}{\partial z} \quad (4.3)$$

Continuity equation:

$$\frac{\partial u}{\partial x} + \frac{\partial v}{\partial y} + \frac{\partial w}{\partial z} = 0 \tag{4.4}$$

Conservation of heat:

$$\frac{\mathrm{d}T}{\mathrm{d}t} = \frac{\partial T}{\partial t} + u\frac{\partial T}{\partial x} + v\frac{\partial T}{\partial y} + w\frac{\partial T}{\partial z} = F_T + D_T \tag{4.5}$$

Conservation of salt:

$$\frac{\mathrm{d}S}{\mathrm{d}t} = \frac{\partial S}{\partial t} + u\frac{\partial S}{\partial x} + v\frac{\partial S}{dy} + w\frac{\partial S}{\partial z} = F_S + D_S \tag{4.6}$$

where (x, y, z) is Cartesian space, t is time, (u, v, w) the three components of velocity, f is the Coriolis parameter, ρ_0 the mean ocean density, p is pressure, ρ is density, g is gravity, T is potential temperature and S salinity. The terms denoted by F and D represent, respectively, forcing and dissipation terms, discussed below. The Coriolis parameter $f = 2\Omega \sin\phi$ where Ω is the angular velocity of the Earth's rotation ($7.3 \times 10^{-5}\,\mathrm{sec}^{-1}$) and ϕ is latitude. T, the potential temperature (often also denoted as θ), is the temperature a given fluid element would have if it were moved to a fixed reference pressure (normally the sea surface). This quantity is approximately a conserved property, unlike *in situ* temperature. Density ρ is a function of potential temperature θ, salinity S and pressure p through the non-linear Equation of State [see Gill (1982) appendix for details].

The configuration of an ocean model involves solving (4.1)–(4.6) for u, v, w, p, T and S over a given grid. The spatial-scale of the grid chosen determines to what extent various processes are resolved. Motion in the ocean occurs at a variety of scales, from molecular diffusion processes (scales of 10^{-6} metres) right through to oceanic gyres (scales of 10^{7} metres).

Figure 4.6 shows these processes as a function of spatial extent. It turns out that a significant component of oceanic energy resides at the scale of the external Rossby radius R, which is the length-scale at which rotation effects are as important a restoring force on motion as gravitational (or buoyancy) effects.

$$R = \sqrt{gh}/|f| \tag{4.7}$$

where h is the depth of the ocean. Oceanic eddies are typically of the scale of the external Rossby radius. R varies from around 100 km at tropical latitudes down to 10 km at high latitude. Coarse resolution ocean models adopt spatial grids of increment $\approx 100 - 400$ km, well above the Rossby radius of deformation. In such models, mesoscale eddy effects must be parameterized in some way (discussed below).

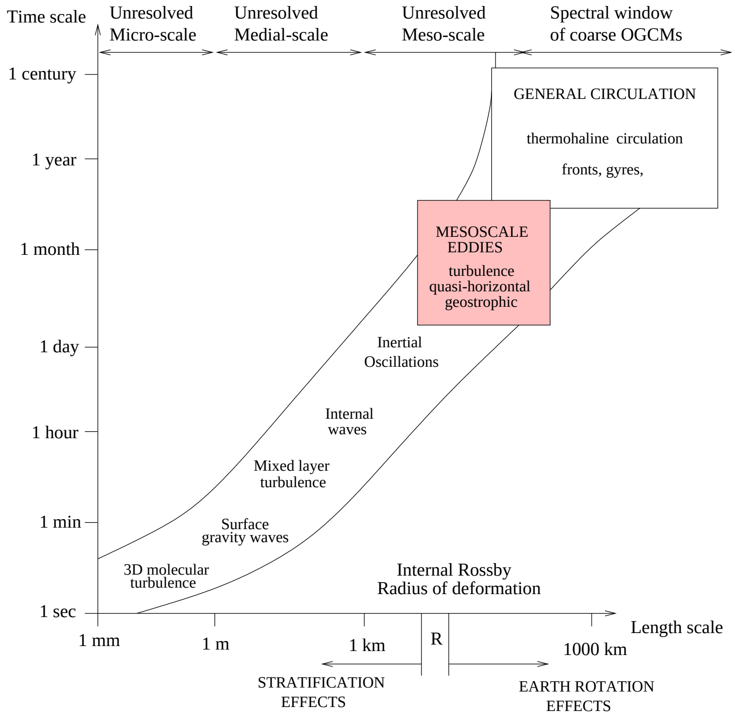

Fig. 4.6. Types of motion in the ocean as a function of spatial extent (from Mathieu, 1999).

4.3.2 Model Choice of Vertical Coordinate

Ocean modellers adopt a variety of numerical techniques for the treatment of the vertical coordinate. The three most common vertical schemes used in large-scale ocean models are depicted in Fig. 4.7. The first one uses geopotential or horizontal z-levels, reducing the observed bathymetry to a series of steps (e.g., MOM, DieCast). The second uses isopycnal layers as the vertical coordinate system, where the layer-averaged velocities and layer-thicknesses are the dependent variables (e.g., MICOM). The third uses a terrain-following sigma-coordinate system through the transformation of the water column depth from $z = 0$ to the bottom into a uniform depth ranging from 0 to 1 (e.g., POM, SPEM).

Each vertical coordinate system has its own advantages and disadvantages. The "z-level" model is flexible in a number of applications and lowest in computational requirements, although its grid orientation can result in excessive diapycnal mixing. In addition, downslope plume flows normally require some form of parameterisation to preserve water-mass signatures. Similarly, upwelling through thin bottom boundary layers in coastal regions is

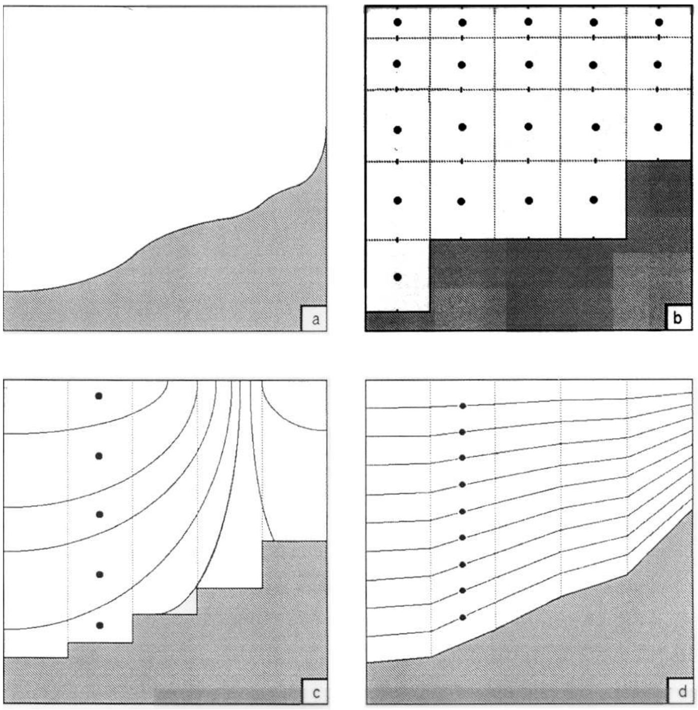

Fig. 4.7. The three most common vertical schemes used in large-scale ocean models (**a**) Observed bathymetry; (**b**) z-level model topography; (**c**) isopycnal layer; and (**d**) sigma-coordinate topography (from DYNAMO, 1997).

not well resolved by z-level models. Isopycnal layer models are ideal for simulating water-mass spreading and eliminating unphysical diapycnic mixing, although the use of single potential density values is dynamically inconsistent and can lead to errors in high latitude water mass distributions. The sigma-coordinate, with terrain-following levels, is most likely to realistically capture bottom boundary flows, such as bottom water plumes. Its coordinate is ideal for flow dominated by topographic effects, although it can result in excessive diapycnic mixing near strong topographic or isopycnal slopes. Sigma-coordinate models also require strongly smoothed bathymetry or high horizontal resolution to avoid numerical errors associated with the calculation of the pressure gradient terms.

4.3.3 Subgrid-scale Processes and Dissipation

Given the enormous range of spatial scales apparent in ocean circulation processes (order 10^{12}), all ocean models need to treat subgrid processes to some degree. For coarse resolution models, this includes mesoscale eddies and their effect on the large-scale flow.

The dissipation or mixing of momentum in the ocean is required to balance the continual input of mechanical wind energy at the air-sea interface. Kinetic energy in the ocean is transferred from large-scales to smaller scales (eventually molecular). The standard approach to parameterising the mixing of momentum is to relate the subgrid-scale dissipation to large-scale properties of the flow via a Fickian equation of the form

$$D_u = \frac{\partial}{\partial x}\left(A_H \frac{\partial u}{\partial x}\right) + \frac{\partial}{\partial z}\left(A_V \frac{\partial u}{\partial z}\right) \tag{4.8}$$

$$D_v = \frac{\partial}{\partial y}\left(A_H \frac{\partial v}{\partial y}\right) + \frac{\partial}{\partial z}\left(A_V \frac{\partial v}{\partial z}\right) \tag{4.9}$$

$$D_w = \frac{\partial}{\partial z}\left(A_V \frac{\partial w}{\partial z}\right) \tag{4.10}$$

where A_H, A_V are the horizontal/vertical eddy viscosity coefficients, respectively. Typically ocean modellers adopt values for A_H, A_V that greatly exceed their estimated magnitude to avoid numerical instabilities. Under a hydrostatic assumption, as typically used in coastal and larger scale models, D_w is considered negligible compared to ρg [as per (4.3)]. The horizontal viscosity terms represent a very ad-hoc parameterisation for the exchange of horizontal momentum from sub-grid scales up to the model grid-scale. The term is required to maintain numerical stability as the viscosity approximation acts to dissipate energy, without causing spurious sources of momentum. The most common approach is a Laplacian operator.

An example of a flow and resolution-dependent parameterization for A_H is

$$A_H = C \Delta x \Delta y \frac{1}{2}\left(\left[\frac{\partial u}{\partial x}\right]^2 + \left[\frac{\partial v}{\partial x} + \frac{\partial u}{\partial y}\right]^2 + \left[\frac{\partial v}{\partial y}\right]^2\right)^{\frac{1}{2}}$$

where C is the Smagorinsky constant (typically < 0.2) and $\Delta x, \Delta y$ are the horizontal grid spacings. This formulation determines A_H as a function of grid resolution and horizontal velocity gradients (e.g., Smagorinsky, 1963). For coastal applications with high horizontal resolution, A_H is often set to small constant values [e.g., for $\Delta x = 0.5\,\mathrm{km}$, $A_H = 2\,\mathrm{m^2 s^{-1}}$ (Allen et al., 1995)]; whereas for coarser horizontal resolution, A_H can have magnitudes of the order of 10 to 100 $\mathrm{m^2 s^{-1}}$.

For different applications the vertical eddy viscosity A_V must be suitably defined in order to adequately model factors such as the frictional effects of the wind on the ocean surface, and the frictional drag associated with flow over the ocean floor. Many applications assume that A_V is constant in space and time [e.g., in most coarse global models, with $A_V \simeq 2 \times 10^{-3}$ m^{2}s^{-1} (Toggweiler et al., 1989; England, 1993)]. Others assume that A_V does not change with time but varies over the water column according to some predefined shape function (e.g., Lentz, 1995), while still others parameterise A_V as a function of the stability of the water column (e.g., Pacanowski and Philander, 1991; Mellor and Yamada, 1982). This aspect of ocean modelling remains uncertain since modellers are trying to capture the effects of processes that occur on scales of the order of centimetres to metres using vertical grids that have scales of the order of 10–1000 m.

Viscosity processes in the horizontal occur on scales of 10's to 100's of kilometres, such as mixing by eddies, whereas in the vertical, they are dominated by vertical shear instabilities, convective overturning and breaking internal waves over rough bathymetry. This accounts for viscosity coefficient values with $A_H \approx 10^6 A_V$. This is to ensure numerical stability, and given that model simulations are relatively insensitive to this parameter, few other approaches have been tested. An exception is the argument by Holloway (1992) that the ocean, in the absence of momentum input from the wind, would spin down not to a state of rest but to a state of higher system entrophy. This is because eddies interacting with bottom topography can exert a large-scale systematic force on the mean ocean circulation. Under this so-called "topographic stress" parameterisation, the horizontal viscosity terms of (4.8)–(4.9) are rewritten with (u, v) replaced by $(u - u_*, v - v_*)$, where (u_*, v_*) represent the maximum entropy solution velocities (see Holloway, 1992; Eby and Holloway, 1994 for further details).

The mixing of scalars (such as T, S, and chemical tracers) has received much attention in recent years. The traditional formulation for subgrid-scale tracer mixing adopted by Bryan (1969) and Cox (1984) was of the form

$$D_t = \frac{\partial}{\partial x}\left(K_H \frac{\partial T}{\partial x}\right) + \frac{\partial}{\partial y}\left(K_H \frac{\partial T}{\partial y}\right) + \frac{\partial}{\partial z}\left(K_V \frac{\partial T}{\partial z}\right) \tag{4.11}$$

with a similar equation for salinity. Here, K_H, K_V are the eddy diffusivities in the horizontal/vertical directions. Normally K_H, K_V are taken to be either constant or some simple depth-dependent profile (e.g., Bryan and Lewis, 1979). Like the viscosity coefficients, K_H and K_V are typically chosen to ensure numerical stability with $K_H \approx 1 \times 10^7$ m^{2}s^{-1} and $K_V \approx 0.2 - 1.0 \times 10^{-4}$ m^{2}s^{-1}. In the real ocean, however, mesoscale eddies are known to diffuse scalars more efficiently *along* surfaces of constant potential density. The work involved in mixing tracers *across* density surfaces is order $10^6 - 10^7$ more than that required to stir *along* density surfaces. Thus, high horizontal eddy diffusivities will be unrealistic in regions of steeply sloping density surfaces. England (1993), Hirst and Cai (1994) and others have demonstrated the problems of using strictly Cartesian mixing coefficients in regions such as the Southern Ocean. Model artifacts include unrealistic water-mass blending, spurious vertical velocities and excessive poleward heat transport across the ACC.

A solution to the problem of tracer mixing in ocean models was first proposed by Redi (1982) and implemented by Cox (1987), wherein the eddy diffusivity tensor $K_{H,V}$ was oriented along density surfaces rather than in a Cartesian system. However, to ensure numerical stability, this so-called "isopycnal mixing" scheme originally required a background horizontal diffusivity, meaning that whilst it simulated increased isopycnal mixing, it also maintained some spurious horizontal diffusion. Theoretical developments in more recent studies have identified solutions to this problem. One solution is to construct a model grid that orients its surfaces along isopycnals rather than along a Cartesian coordinate system (e.g., Bleck et al., 1992). Such models have now been configured over global domains and have quite successfully captured the ocean's thermohaline circulation and climate processes (e.g., Bleck et al., 1997; Sun, 1997).

Mesoscale eddies affect tracers not only by increasing mixing rates along density surfaces, but also by inducing a larger-scale transport rather like an adiabatic advection term (e.g., Rhines, 1982; Gent and McWilliams, 1990; McDougall, 1991). Gent and McWilliams (1990) and later Gent et al. (1995) proposed a parameterization for this process wherein the large-scale density field is used to estimate the magnitude of the eddy-induced advection, (u_*, v_*), namely:

$$u_* = \frac{\partial}{\partial z}\left(K_e \frac{\partial\rho/\partial x}{\partial\rho/\partial z}\right) \tag{4.12}$$

$$v_* = \frac{\partial}{\partial z}\left(K_e \frac{\partial\rho/\partial y}{\partial\rho/\partial z}\right) \tag{4.13}$$

and since the eddy-induced advection field is non-divergent (Gent et al., 1995), w_* can be derived from the equation

$$\frac{\partial u_*}{\partial x} + \frac{\partial v_*}{\partial y} + \frac{\partial w_*}{\partial z} = 0$$

yielding

$$w_* = \frac{\partial}{\partial x}\left(K_e \frac{\partial\rho/\partial x}{\partial\rho/\partial z}\right) + \frac{\partial}{\partial y}\left(K_e \frac{\partial\rho/\partial y}{\partial\rho/\partial z}\right) \tag{4.14}$$

It turns out that the Gent et al. (1995) mixing scheme results in a positive definite sink, on the global mean, of available potential energy. This means that model runs of coarse resolution can be integrated with zero background horizontal diffusion and yet remain stable, as the Gent et al. (1995) advection terms act as a viscosity or dissipative term on the model scalar properties. Successful simulations with zero K_H have been achieved with minimal numerical problems (see Hirst and McDougall, 1996; England and Hirst, 1997).

Recent estimates of vertical diffusion rates show very low values ($\approx 0.1\,\mathrm{cm}^2\mathrm{s}^{-1}$) in the upper ocean, elevated values near regions of rough bottom bathymetry (up to $10\,\mathrm{cm}^2\mathrm{s}^{-1}$) and much weaker values in the ocean interior over regions of smooth bottom bathymetry such as abyssal plains (Ledwell et al., 1998; Polzin et al., 1997). Models have traditionally adopted constant or simple depth-dependent profiles of K_V. Unfortunately, key ocean model parameters such as the meridional overturn and poleward heat transport are controlled to a large extent by the magnitude of K_V (e.g., Bryan, 1987). Recent efforts have been made to estimate K_V as a function of bottom bathymetry roughness and ocean depth in global ocean models (e.g., Hasumi and Suginohara, 1999). It turns out the meridional overturn and poleward heat transport in an ocean model can be vigorous with zero K_V over the ocean interior and only enhanced K_V over rough terrain (e.g., Marotzke, 1997). This gives increased confidence in the capacity of ocean models to realistically capture the large-scale ocean circulation without fully resolving smaller-scale physical processes.

In most applications of coastal and tropical ocean models, flow-dependent vertical mixing schemes are used to represent enhanced mixing in the frictional surface and bottom boundary layers. These schemes are typically dependent on the local Richardson number:

$$Ri = \frac{N^2}{(\partial \bar{u}/\partial z)^2}$$

where $N^2 = \dfrac{g}{\rho_0}\dfrac{\partial \rho}{\partial z}$ is the buoyancy frequency, and $\bar{u}$ the mean horizontal flow speed. As such, Ri quantifies the vertical stability of the water column in relation to the velocity shear. Examples of Richardson number dependent schemes are described in detail by Mellor and Yamada (1982), Pacanowski and Philander (1991) and Kantha and Clayson (1994) to name a few.

It is now known that significant vertical mixing occurs over rough bottom bathymetry as barotropic tides agitate internal wave breaking (e.g., Toole et al., 1997). Future parameterizations of K_V should take account of global tidal flow fields and bathymetry roughness in order to incorporate these effects in some way.

Another subgrid-scale oceanic process is vertical convection, wherein surface buoyancy loss (via cooling, evaporation, or sea-ice formation) leads to vertically unstable waters and overturn to depths up to 1000 m or so. Examples include Mode Waters (McCartney, 1977), 18°C water in the North Atlantic (Worthington, 1976), and Weddell Sea Bottom Water. Since convection is intimately tied to water-mass formation, representing it in ocean models is critical. Because the horizontal scale of convection is order kilometres, no greater than its vertical scale, non-hydrostatic processes are involved. Present parameterisations of vertical convection simply mix $T-S$ and other scalars completely over the unstable portion of the water column, removing the vertically unstable layer outside any calculation of vertical motion. Model simulations of nonhydrostatic convection by Send and Marshall (1997) indicate that to first order this vertical mixing approach approximates the integral effects of vertical convection on the simulated $T-S$ fields. The problem remains, however, that the horizontal extent of convection in coarse resolution models is necessarily at least the dimension of a model grid box, which can be about 100–400 km.

4.3.4 Boundary Conditions and Surface Forcing

Ocean models have to be given explicit boundary conditions for motion and temperature-salinity (see also Fig. 4.5). These include boundary conditions at the air-sea interface, bottom boundary conditions (for momentum), as well as lateral boundary conditions for regional models. Side boundary conditions at land masses are the most simple, including no-slip non-normal flow, and zero fluxes of heat and salt. In coarse models, bottom boundary layers normally adopt some simple relationship to approximate the effects of frictional drag on the deep ocean flow (see, for example, Toggweiler et al., 1989).

Surface forcing is a crucial aspect of boundary conditions in ocean models. Firstly for motion, modellers may choose between a "rigid-lid" approximation and a free surface condition. Under the rigid-lid approximation, the vertical velocity w is zero at the sea surface, thereby excluding surface gravity waves and allowing a longer model time step (Bryan, 1969). This means further that the total volume of the ocean remains constant and that freshwater fluxes across the air-sea interface must be represented as effective salt fluxes. Other surface pressure gradients, such as those due to large scale geostrophic flow, are allowed under a "rigid-lid" approximation, but not predicted directly. The free surface condition, on the other hand, carries sealevel height or pressure as a prognostic variable, thereby eliminating the need to predict the barotropic velocity field [which becomes costly in a domain of high resulution (Dukowicz and Smith, 1994)]. Techniques have emerged to handle a free surface condition without significantly shortening the model time step; either by using many small steps in time for solving the free-surface during each single time-step of the full 3D model (Killworth et al., 1991), or by solving the free-surface equations using an implicit method (Dukowicz and Smith, 1994). Benefits of adopting these approaches include improved computational efficiency in high resolution domains, an ability to model ocean flow over unsmoothed topography, and a natural prognostic variable for assimilation of satellite height data into ocean models (see, e.g., Stammer et al., 1996).

Surface forcing fields are required in ocean models for momentum, temperature and salinity [for an excellent review on these topics, see Barnier (1998)]. Surface pressure and barotropic motion will adjust freely to the model simulated $T-S$ and 3D motion, so direct surface forcing fields are not required.

Tidal forcing is also required when sub-diurnal scales of motion are important, such as for coastal ocean models or for flow in harbours and bays. Momentum input into the oceans is via mechanical wind forcing, normally expressed as a wind stress vector τ, where

$$\tau = \rho_a c_D |U_{10} - U_W| \mathbf{u}_{10} \tag{4.15}$$

with ρ_a the density of air, c_D a turbulent exchange drag coefficient, U_{10} the wind speed at anenometer height, 10 m above the ocean surface, U_W the ocean current speed at the sea surface, and $\mathbf{u}_{10}$ the wind velocity at anenometer height. This wind-stress is then converted into a forcing term in the momentum equations (4.1)–(4.2) via the expression

$$F_{u,v} = \frac{\partial}{\partial z}(\tau/\rho_0) \qquad \text{at} \quad z = 0 \tag{4.16}$$

Direct observations of wind stress over the ocean are relatively sparse, though a number of long-term global climatologies exist (e.g., Hellerman and Rosenstein, 1983), as well as others derived from more recent remote sensing technologies (e.g., Bentamy et al., 1997). Another technique for model wind forcing is to adopt output from numerical weather prediction models (NWPs); normally these products are derived from a combination of observations and forecasts via data assimilation (e.g., Kalnay et al., 1996; Gibson et al., 1997). The advantage of NWP products is that they have global high density coverage, use available observations, and are dynamically consistent. They are, in addition, provided in real time which facilitates ocean hindcasting.

Surface forcing conditions for temperature (T)–salinity (S) in ocean models can be formulated in a number of ways. The equations are [refer to (4.5) and (4.6)]:

$$F_T = \frac{Q_{\text{net}}}{\Delta z_1 \rho_0 c_p} \tag{4.17}$$

$$F_S = \frac{S_0}{\Delta z_1}(E - P - R) \tag{4.18}$$

where Q_{net} is the net heat flux into the surface layer (W m^{-2}), Δz_1 is the upper model level thickness, ρ_0 density of seawater, c_p the specific heat of seawater, S_0 mean ocean salinity, E evaporation rate, P precipitation rate, and R river run-off rate (E, P and R are all in m s^{-1}). The value S_0 is required to convert the net freshwater flux into an equivalent salt flux in rigid-lid models [see Barnier (1998) for further details]. So, in formulating heat and salt fluxes, ocean modellers require some knowledge of Q_{net}, E, P and R. Q_{net} is comprised of several components;

$$Q_{\text{net}} = Q_{\text{SW}} - Q_{\text{LW}} - Q_{\text{LA}} - Q_{\text{SENS}} - Q_{\text{PEN}} \tag{4.19}$$

where Q_{SW} is the net shortwave radiation entering the ocean, Q_{LW} is the net longwave radiation emitted at the air-sea interface, Q_{LA} is the latent heat flux, Q_{SENS} is the sensible heat flux, and Q_{PEN} the penetrative heat flux from the base of model level 1 into model level 2.

The Q_{PEN} term can generally be neglected except when shallow surface layers are adopted (e.g., Godfrey and Schiller, 1997). Bulk formulae can be used to estimate the heat flux components of (4.19) (e.g., Barnier, 1998), in particular, Q_{SW} depends on latitude, time of year, cloud cover and surface albedo; Q_{LW} depends primarily on ocean surface temperature, Q_{LA} and Q_{SENS} depend on surface wind speed, humidity (for Q_{LA}), and air-sea temperature difference. Satellite and *in situ* observations of these variables can be used to construct bulk estimates of heat and freshwater fluxes across the air-sea interface.

Unfortunately many of these quantities are only sparsely observed over the ocean, and in addition they are characterised by high-frequency variability, making it extremely difficult to construct long-term climatologies. Also, variables such as precipitation and evaporation are not easily quantified using satellite technologies. Nevertheless, a number of global heat and freshwater flux climatologies exist (e.g., Esbenson and Kushnir, 1981; Josey et al., 1999; Baumgartner and Reichel, 1975). Unfortunately, direct forcing with these fluxes can lead to significant model errors (e.g., Moore and Reason, 1993), as small errors in fluxes can accumulate into large errors in model $T-S$ over a sufficient period of integration time. Because of this, large-scale ocean modellers have commonly adopted grossly simplified formulations of thermohaline forcing, for example, restoration to observed surface T and S:

$$F_T = \gamma_T \left(T_{\mathrm{obs}} - T_{\mathrm{model}}\right) \tag{4.20}$$

$$F_S = \gamma_S \left(S_{\mathrm{obs}} - S_{\mathrm{model}}\right) \tag{4.21}$$

where γ_T, γ_S are time-constants determining how long heat/salinity anomalies persist before they are damped by air-sea forcing, (T_{obs}, S_{obs}) are the observed climatological $T-S$, and (T_{model}, S_{model}) the model surface $T-S$. Haney (1971) justified this style of formulation for temperature so long as T_{obs} is replaced by T_{EFF}, where T_{EFF} is the temperature the ocean would obtain if there were no heat transported by it. Various techniques exist to estimate the distribution of T_{EFF} (e.g., Rahmstorf and Willebrand, 1995; Cai and Godfrey, 1995). There is, however, no such justification for salinity, as salinity at the sea-surface has no significant role in controlling air-sea freshwater fluxes. This lead many modellers to use so-called "mixed boundary conditions", (e.g., Bryan, 1987; Weaver et al., 1991), wherein a model run is integrated with restoring salinity conditions, diagnosed for the effective salt flux distribution, and re-run with this flux condition on S; thereby allowing the model to exhibit variability in S independent of the surface forcing fields. More recently, the Haney (1971) heat flux formulation has been extended to include simple parameterizations for the atmospheric dispersion of ocean heat anomalies (Rahmstorf and Willebrand, 1995; Power and Kleeman, 1994), to allow, for example, the simulation of oceanic variability otherwise suppressed by a boundary condition of the form in (4.20).

Data sets for surface thermohaline forcing include flux climatologies (refer to citations above and Woodruff et al., 1987, DaSilva et al., 1994), re-analyses of NWP simulations (e.g., Barnier et al., 1995; Béranger et al., 1999; Garnier et al., 2000) and satellite derived data products (e.g., Darnell et al., 1996). However, in practical terms, any direct flux forcing technique can lead to substantial errors in simulated $T - S$ because of possible model bias and errors in the flux fields themselves. For example, an error in heat flux as small as 1 W m^{-2} (which is at least an order of magnitude less than the typical error associated with heat flux climatologies) would result in an error in upper level T of 7.5°C after 50 years of run time (assuming a surface level of thickness 50 m). To address this problem, it is becoming common practice for modellers to adopt surface thermohaline forcing of the form

$$F_T = \frac{Q_{\text{net}}}{\Delta z_1 \rho_0 c_p} + Q_{\text{CORR}}$$

and

$$F_S = \frac{S_0}{\Delta z_1}(E - P - R) + S_{\text{CORR}} \tag{4.22}$$

with

$$Q_{\text{CORR}} = \gamma_T \left(T_{\text{obs}} - T_{\text{model}}\right)$$

$$S_{\text{CORR}} = \gamma_S \left(S_{\text{obs}} - S_{\text{model}}\right)$$

corresponding to the Newtonian restoring terms described earlier in (4.20) – (4.21).

Typically, these heat flux and salt flux correction terms adopt time-scale values for γ_T, γ_S that give weak restoring towards observed $T - S$, thereby enabling thermohaline variability (see also Wood et al., 1999).

Lateral boundary conditions in regional ocean models represent a major area of uncertainty in ocean modelling. In order to resolve oceanic features with scales of the order of kilometres to 10's of kilometres, high horizontal resolution is required. However, limited computational resources mean that global coverage at such resolution is not feasible. Therefore either regional models have to be nested inside global models, where the global model provides boundary conditions for the regional model, or open boundary conditions must be incorporated into the regional model. Open boundary conditions generally assume limited physics at the boundary. There are several detailed studies on open boundary conditions (e.g., Orlanski, 1976; Chapman, 1985; Palma and Matano, 1997), where most attempt to represent the advection or propogation of modelled disturbances into or out of the domain. These conditions are referred to as passive conditions since they are designed to have minimal impact on the model solution. Often sponge layers (Chapman, 1985), which are designed to slow model disturbances down near open boundaries, are employed in order to further reduce any unwanted reflection. For cases where a typical state at the boundary is known or assumed, e.g. tidal flows, non-passive boundary conditions are often used, where a relaxation term is added to the passive conditions mentioned above (e.g., Flather, 1976; Blumberg and Kantha, 1985). Many applications relax temperature and salinity to their climatological values (e.g., Stevens, 1991; Gibbs et al., 1997; Oke and Middleton, 2001), with velocities being relaxed to their geostrophic boundary values that match the $T-S$ climatology at the boundary. Barotropic boundary flows may be estimated using a Sverdrup relationship. The uncertainty associated with the choice of open boundary condition means that a substantial amount of testing and model validation should be performed before confidence is shown in a regional simulation.

The above discussions of ocean model forcing are in the context of "ocean-only" model integrations. However, even when coupling to an atmospheric GCM, some integration of an ocean-only model is required prior to coupling. In that case, a number of spin-up strategies are possible (as discussed by Moore and Reason, 1993). This is detailed further in Chap. 2.

4.4 Some Commonly Used Ocean Models

There are a vast number of ocean models used around the world today. Some of these models are designed for a very specific use, limited to a certain geographic region and only resolving the dominant components of the equations of motion. Other more generalised models have been configured to be operational over a range of space and time-scales with a variable geographic domain. Such models are becoming widely used with literally hundreds of applications across many institutions. A limited set of such ocean models are described here.

4.4.1 The GFDL Modular Ocean Model

The GFDL Modular Ocean Model (MOM) is the most widely used ocean model in large-scale coupled climate simulations. It is a finite difference realisation of the primitive equations governing ocean circulation. These equations are formulated in spherical coordinates. An identifying feature of the GFDL model is that it is configured with its vertical coordinate as level geopotential surfaces (i.e., so-called z-level). The MOM grid system is a rectangular Arakawa staggered B grid. Further model details can be found in Pacanowski (1995) and Bryan (1969). Applications range from global at coarse and eddy-resolving resolution, down to regional and idealised process-oriented models. A full bibliography of MOM-related papers appears in an appendix in Pacanowski (1995).

As an example, Figure 4.8 shows the upper ocean circulation in the South Pacific Ocean from such a model (from England and Garçon, 1994). This model has resolution and geometry typical of state-of-the-art coupled ocean-atmosphere models used to study climate variability and anthropogenic climate change. The resolution is coarse (1.8 degrees in longitude and 1.6 degrees in latitude) so the eddy field is not resolved explicitly. There are 33 unequally spaced vertical levels with bottom topography and global continental outlines as realistic as possible for the given grid-box resolution. The model is driven by Hellerman and Rosenstein (1983) winds. The model temperature and salinity are relaxed to the climatological annual mean fields of Levitus (1982) at the surface. The figure shows vectors of ocean currents simulated at 70 m depth, with topography shallower than 3000 m depth shaded. Apparent is the bathymetric steering of the Antarctic Circumpolar Current (ACC), even in the upper ocean well above the main topographic features in the region.

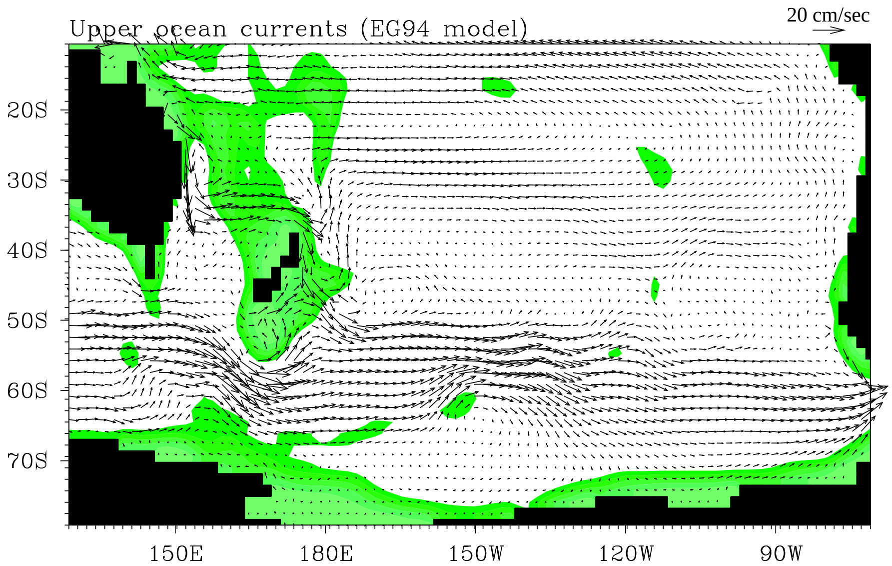

Fig. 4.8. Upper ocean circulation in the South Pacific Ocean, from England and Garçon (1994). Topography features shallower than 3000 m are shaded.

The tendency for flow in the ACC to be along constant depth contours is not difficult to understand. The reason for this is that the flow is mostly barotropic so that the potential vorticity

$$Q = \frac{\zeta + f}{h + \eta}$$

will be conserved, where ζ is the relative vorticity, f the Coriolis parameter or planetary vorticity, h the ocean depth and η is the relative sealevel elevation. At the latitude of the ACC, apart from mesoscale eddies, the large-scale flow is such that its relative vorticity $\zeta << f$. In addition, sealevel variations are of the order of $\simeq 1 - 2$ metres compared with an ocean depth of $h \simeq 2000 - 4000$ metres. So the conservation of potential vorticity implies that $f/h \simeq$ constant. With the ACC flow being primarily west to east we can take f as approximately constant, so a fluid column tends to have the same value of depth h and is thus steered along isobaths.

4.4.2 The Princeton Ocean Model

The Princeton Ocean Model (POM) adopts curvilinear orthogonal coordinates and a vertical sigma-coordinate to facilitate simulations of coastal zone flows (Mellor, 1998). The horizontal time-differencing is explicit whereas the vertical differencing is implicit, allowing a fine vertical resolution in the surface and bottom layers. This is important in coastal ocean models as the near-shore ocean can be a region of substantial surface and bottom boundary gradients. POM can be integrated with a free-surface and using split time-stepping (as in MOM). Another positive feature of the POM is the embedded turbulence sub-model (Mellor and Yamada, 1982), which is designed to provide realistic, flow-dependent vertical boundary layer mixing. This sub-model, along with the terrain-following sigma-coordinates, allows the modeller to resolve bottom boundary layer flows that are often associated with coastal upwelling, a feature that z-level models cannot adequately represent. Applications of the POM range from coastal (Mellor, 1986) through to regional (Middleton and Cirano, 1999) and basin-scale studies (Ezer and Mellor, 1997).

An example of the POM configured with idealised continental shelf and slope topography, and forced with constant (0.1 Pa) upwelling favourable winds is shown in Fig. 4.9 (taken from Oke and Middleton, 1998). This figure shows the evolution of a cross-shelf slice of temperature, alongshelf velocity and cross-shelf streamfunction over a 15-day period. This sequence shows the initial response to the wind in the streamfunction field, where an upwelling circulation is generated. By Day 5 a coastal jet has formed in the direction of the wind and isotherms have been upwelled to the surface. By Day 10 the upwelling is concentrated in the bottom boundary layer, as indicated by the concentration of the cross-shelf streamlines over the topography, and the upwelling front has been advected off-shore. This type of idealised configuration modelling has given oceanographers great insight into the overall dynamics of coastal upwelling (e.g., Allen et al., 1995), as it may enable the upwelling dynamics to be isolated from more complicated continental shelf processes, such as the effects of topographic variations.

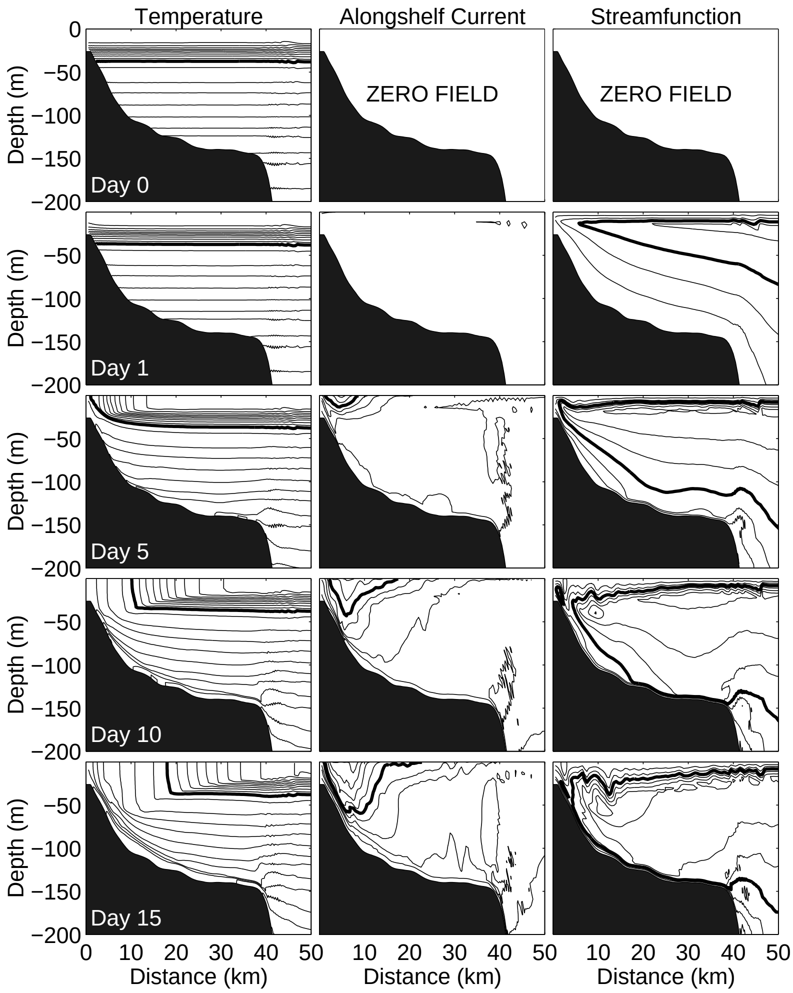

Fig. 4.9. A sequence of cross-shelf slices of temperature, along-shelf velocity and cross-shelf streamfunction (left-right; contour intervals = 0.5°C, $0.1\,\mathrm{m\ s^{-1}}$, $0.1\,\mathrm{m^2 s^{-1}}$ respectively) showing their evolution in response to constant ($0.1\,\mathrm{Pa}$) upwelling favourable winds (Oke and Middleton, 1998).

4.4.3 The Miami Isopycnic Coordinate Model (MICOM)

MICOM is a primitive equation "isopycnic" ocean model that uses equations that have a coordinate of potential density in the vertical direction (Fig. 4.7c) instead of the traditional vertical coordinate of depth. That is, whereas z-level and sigma coordinate models predict the density at a fixed depth, MICOM predicts the depths at which certain density values are encountered. Thus, the traditional roles of water density and height as dependent and independent variables are reversed. The surface mixed layer (with different isopycnal values) sits over the subsurface isopycnic domain. The horizontal coordinate system is the Arakawa C grid. The model accommodates a user specified, horizontal geographic zone. Further model details can be found in Bleck et al. (1992). Recently, MICOM has been configured for global ocean simulations (Bleck et al., 1997). A map of the simulated surface ocean currents from a 2-degree by $2\cos(\phi)$-degree global MICOM simulation (Sun, 1997) is shown in Fig. 4.10.

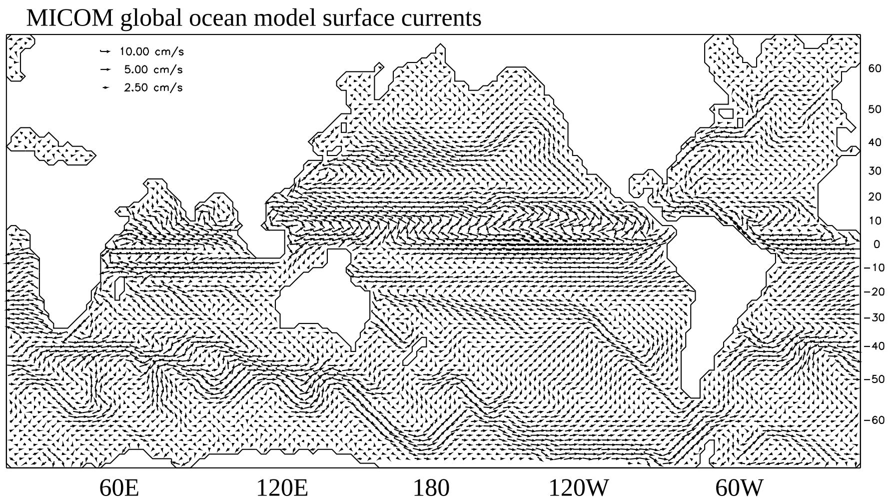

Fig. 4.10. Simulated surface ocean currents from a 2-degree by $2\cos(\phi)$-degree global MICOM simulation (after Sun, 1997).

4.4.4 The DieCast Model

The "DieCast" model is a z-level model like the GFDL MOM, only with different numerical and horizontal grid schemes. The DieCast model combines aspects of the Arakawa A and C grids. DieCast uses fourth order interpolations to transfer data between the A and C grid locations in order to combine the best features of the two grids. This procedure eliminates the A-grid "null space" problems and reduces or eliminates the numerical dispersion caused by Coriolis term integration on the C grid. The modified A grid model includes a fourth order approximation for the baroclinic pressure gradient associated with the important quasi-geostrophic thermal wind. Further discussion of the DieCast grid system is given by Dietrich (1997). The model geometry is in most ways identical to the GFDL MOM. The key difference between DieCast and the GFDL MOM is that DieCast defaults to higher order numerical schemes and incorporates a merged Arakawa A and C grid system, as described above.

4.5 Ocean Model Applications

4.5.1 A Global Coarse Resolution Model

Perhaps the most widely applied global coarse resolution model over the past two decades has been that configured initially by Bryan and Lewis (1979) based on the GFDL Bryan-Cox primitive equation numerical model (Bryan, 1969; Cox, 1984). The Bryan and Lewis (1979) simulation has been used in a wide-ranging series of coupled climate models (e.g., Manabe and Stouffer, 1988, 1993, 1996), ocean-only models used to understand water-mass formation processes (e.g., England, 1992; England et al., 1993; Toggweiler and Samuels, 1992, 1995) and in models of the oceanic carbon cycle (Sarmiento et al., 1998). It has also undergone extensive assessment using geochemical tracers such as radiocarbon (Toggweiler et al., 1989) and chlorofluorocarbons (England et al., 1994; England and Hirst, 1997).

A particular example of the utility of the coarse resolution model of Bryan and Lewis (1979) is exemplified in the England et al. (1993) assessment of the formation mechanism for mode and intermediate waters in the Southern Ocean. Realistic representation of the low-salinity tongue of Antarctic Intermediate Water (AAIW) was achieved by England (1993). He found that the AAIW tongue can quite successfully be simulated provided appropriate attention is taken to observed wintertime salinities near Antarctica, and so long as an isopycnal mixing scheme is incorporated into the model. A diagram showing the observed and modelled salinity is included in Fig. 4.11.

England et al. (1993) found that AAIW is not generated by direct subduction of surface water near the polar front as had been the traditional belief (e.g., Sverdrup et al., 1942). Instead, the renewal process is concentrated in certain locations, particularly in the southeast Pacific Ocean off southern Chile (see Fig. 4.12). The outflow of the East Australian Current progressively cools (by heat loss to the atmosphere and assimilation of polar water, carried north by the surface Ekman drift) and freshens (due to the northward Ekman transport of low salinity Subantarctic Surface Waters) during its slow movement across the South Pacific towards the coast of Chile.

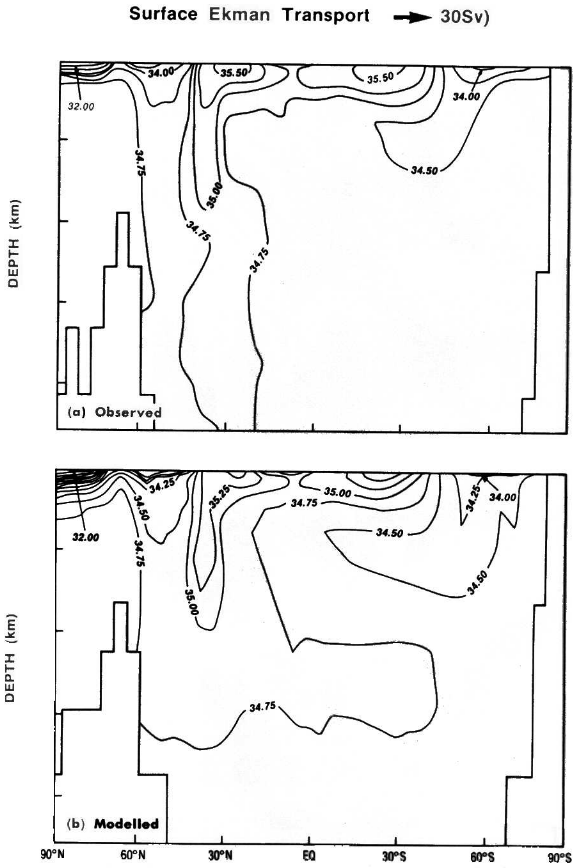

Fig. 4.11. Observed and modelled salinity in the depth-latitude zonal mean. Observations from Levitus (1982), model simulation is that of England et al. (1993).

This results in progressively cooler, denser, and fresher surface water, leading to deeper convective mixed layers towards the east. Off Chile, advection of warmer subsurface water from the north (at 100–900 m depth) enables more convective overturn, resulting in very deep mixed layers from which AAIW is fed into the South Pacific (via the subtropical gyre) and also into the Malvinas Current (via the Drake Passage). This formation mechanism for AAIW was first proposed by McCartney (1977) based on observations; although a detailed dynamical framework was not clear until the England et al. (1993) study.

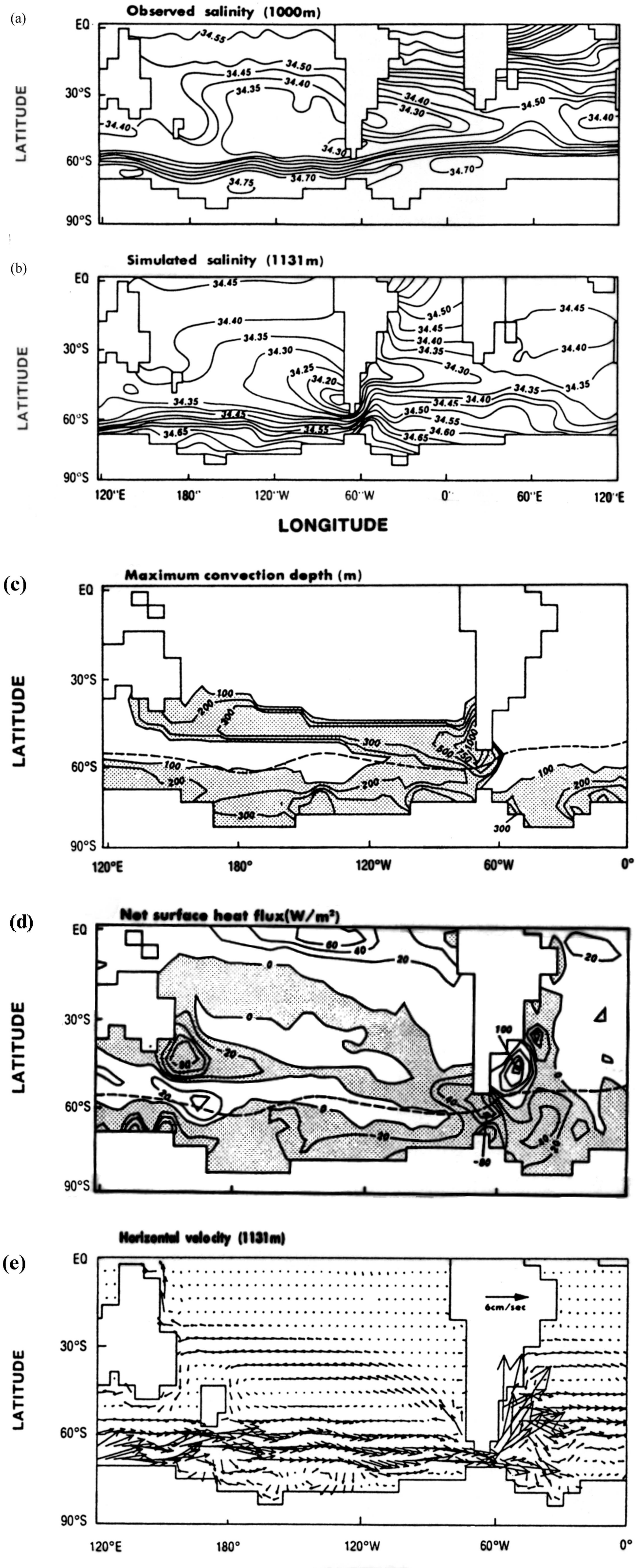

[p]

Fig. 4.12. (**a**) Observed annual-mean salinity at 1000 m depth redrafted from Levitus (1982); (**b**)–(**e**) Simulated properties in the England et al. (1993) ocean model: (**b**) salinity near 1000 m depth; (**c**) net surface heat flux ($W\,m^{-2}$) into the ocean; (**d**) maximum depth (m) of convective overturn; and (**e**) horizontal velocity near 1000 m depth.

4.5.2 Global Eddy-permitting Simulations

The first global domain eddy-permitting ocean model was integrated by Semtner and Chervin (1992). Presently, several groups are moving in this direction, although the huge computational cost of an eddy-permitting global model limits applications to multi-decadal runs. Two prominent examples of global eddy-permitting models include the Ocean Circulation and Climate Advanced Modelling Project (OCCAM) (de Cuevas et al., 1998) and the Parallel Ocean Climate Model (Stammer et al., 1996; Tokmakian, 1996).

The OCCAM project has developed two high resolution (1/4 and 1/8 degree) models of the World Ocean – including the Arctic Ocean and marginal seas such as the Mediterranean. Vertical resolution has 36 depth levels, ranging from 20 m near the surface, down to 255 m at 5500 m depth. OCCAM is based on the GFDL MOM version of the Bryan-Cox-Semtner ocean model but includes a free surface and improved advection schemes. A regular longitude-latitude grid is used for the Pacific, Indian and South Atlantic Oceans. A rotated grid is used for the Arctic and North Atlantic Oceans to avoid the convergence of meridians near the poles. The model was started from the Levitus annual mean $T-S$ fields. The surface forcing uses ECMWF monthly mean winds and a relaxation to the Levitus seasonal surface $T-S$ climatology. This initial model run was integrated for 12 model years. The OCCAM model has been run with high resolution forcing using the six-hourly ECMWF re-analysis data from 1992 onwards. The OCCAM simulation in the region of the Agulhas Retroflection is shown in Fig. 4.13. Agulhas eddies are spawned south of Africa, transporting heat and salt from the Indian Ocean into the Atlantic, contributing to the global transport of properties between ocean basins. This has been linked with the global thermohaline transport of North Atlantic Deep Water (NADW) (Gordon, 1986). Coarse resolution ocean models cannot explicitly resolve oceanic eddies, and so they do not include the heat and salt fluxes associated with Agulhas rings.

The Parallel Ocean Climate Model (POCM) has nominal lateral resolution of 1/4° (Stammer et al., 1996; Tokmakian, 1996). The POCM domain is nearly global running from 75°S to 65°N. The actual grid is a Mercator grid of size 0.4° in longitude yielding a square grid everywhere between the Equator and 75° latitude (Stammer et al., 1996). The resulting average grid size is 1/4° in latitude. Model bathymetry was derived by a grid cell average of actual ocean depths over a resolution of 1/12°. Unlike most coarse models, the fine resolution model includes a free surface (after Killworth et al., 1991) that treats the sea level pressure as a prognostic variable.

The POCM is integrated for the period 1987 through to June 1998 using ECMWF derived daily wind stress fields, climatological monthly mean ECMWF sea surface heat fluxes produced by Barnier et al. (1995), and some additional T, S surface restoring terms. The surface restoring of T and S adopts the Levitus et al. (1994) monthly climatology with a 30-day relaxation time scale. Subsurface to 2000 m depth $T-S$ are also restored towards

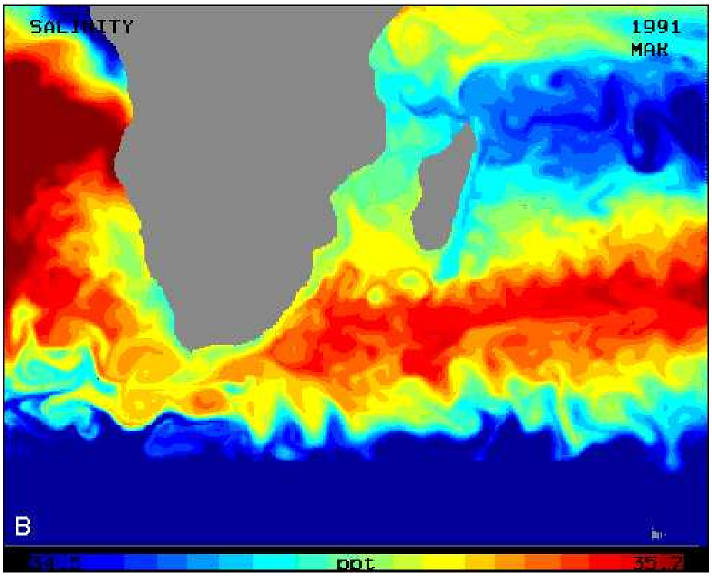

Fig. 4.13. OCCAM simulation of sea surface salinity in the region of the Agulhas Current and leakage into the Indian Ocean (from Semtner, 1995).

Levitus (1982) along artificial model boundaries north of 58°N and south of 68°S to approximate the exchange of water properties with those regions not included in the model domain.

An example of the POCM simulation is shown for the South Atlantic upper ocean in Fig. 4.14. Only velocity vectors at every third grid box are drawn, with no spatial averaging, otherwise the current vectors are difficult to visualise. The Brazil-Falkland confluence is close to the location described from hydrographic and satellite observations. Also, the South Atlantic Current is simulated to the north of the ACC (and separate from it), unlike coarser models which tend to simulate a broad ACC and no distinct SAC. At the tropics, the POCM resolves some of the meridional structure in zonal currents observed (as discussed in Stramma and England, 1999). Eddy-resolving simulations capture much more spatial structure than their coarse resolution counterparts, including more realistic western boundary currents, frontal dynamics, and internal oceanic variability.

4.5.3 Regional Simulations in the North Atlantic Ocean

A large variety of simulations of the North Atlantic Ocean have been carried out within the World Ocean Circulation Experiment (WOCE) Community

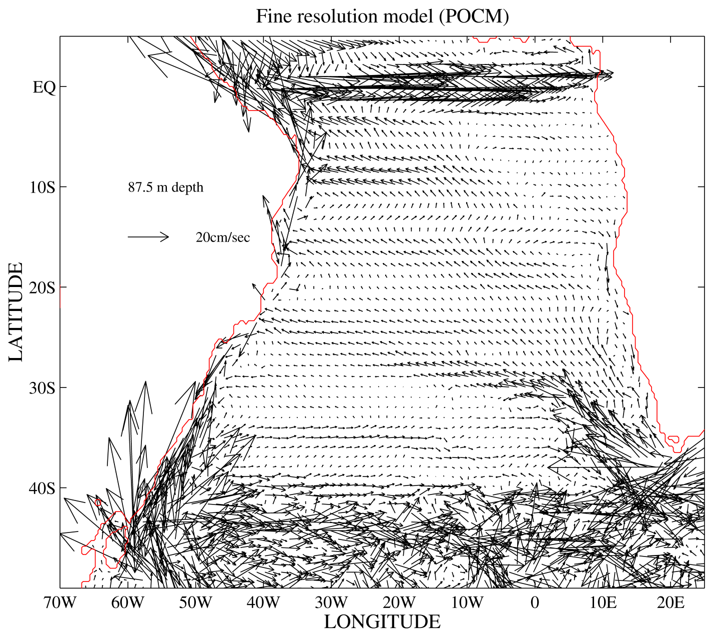

Fig. 4.14. POCM simulation for the South Atlantic upper ocean near 100 m depth (from Stramma and England, 1999). Only velocity vectors at every third grid box are drawn.

Modeling Effort (CME) and more recently by other modelling groups. An overview of some of the CME North Atlantic models is given by Böning et al. (1996), with particular reference to the sensitivity of deep-water formation and meridional overturning to a number of model parameters. It turns out that surface thermohaline forcing (England, 1993), model resolution (Böning et al., 1996), mixing parameterisation (Böning et al., 1995), as well as the resolution of certain subsurface topographic features (Roberts and Wood, 1997) all control model NADW formation rates.

More recently, the Dynamics of North Atlantic Models (DYNAMO) study intercompared a number of simulations in the region using models with different vertical coordinate scheme; namely a model with horizontal z-levels, another with isopycnal layers and thirdly one that used a dimensionless sigma-coordinate (as per Fig. 4.7). The goal of the DYNAMO project was to develop an improved simulation of the circulation in the North Atlantic Ocean, including its variability on synoptic and seasonal time-scales. The study included a systematic assessment of the ability of eddy-resolving models with different vertical coordinates to reproduce the essential features of the hydrographic structure and velocity field between 20°S and 70°N.

Figure 4.15 shows the poleward heat transport in all three ocean models compared with observations. The northward heat transport in the z-level simulation is markedly lower than the observations and the sigma and isopycnal cases south of 40°N. This is due to mixing in the outflow region and spurious upwelling of NADW at midlatitudes (DYNAMO, 1997). On the other hand, the isopycnal run simulates a more realistic heat transport pattern, although its low eddy kinetic energy is compensated by an enhanced deep NADW outflow. Thus, examination of the integral measure of poleward heat transport aliases more subtle dynamical discrepencies in that model. The sigma model also captures a realistic heat transport pattern, although the formation site for NADW is not concentrated in the subpolar region (figure not shown). Overall, the intercomparison of models in the DYNAMO project underscores the relative merits and shortcomings of different vertical coordinates in the context of basin-scale modelling.

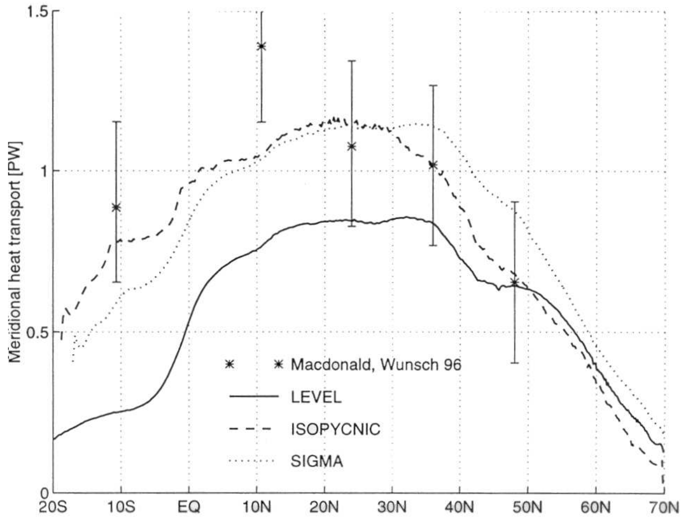

Fig. 4.15. Poleward heat transport in the DYNAMO experiments with z-level, isopycnal and sigma coordinate vertical schemes (from DYNAMO, 1997). Observations are included from McDonald and Wunsch (1996).

4.5.4 ENSO Modelling

Modelling the upper ocean dynamics in tropical waters is crucial for an improved understanding of the El-Niño/ Southern Oscillation (ENSO). ENSO ocean models are ultimately coupled to atmospheric GCMs in order to predict the climate impact of changes in tropical SST. Ocean models used in the context of ENSO simulations have ranged in complexity from shallow water models representing tropical upper ocean dynamics (e.g., Cane and Sarachik, 1977; McCreary, 1976) and modified shallow water models (e.g., Schopf and Cane, 1983), through to three-dimensional general circulation models (e.g., Philander and Pacanowski, 1980). A similar hierarchy of atmospheric models also exists, from those employing simple damped shallow-water dynamics (e.g., Gill, 1980) through to full atmospheric GCMs. In turn, the coupled ocean-atmosphere models used can range from simple models and intermediate coupled models through to 3D coupled GCMs (for a review of the former see Neelin et al., 1998).

Ocean GCMs used to study ENSO dynamics are normally constructed with enhanced horizontal resolution in the tropics, and enhanced vertical resolution in the upper 300–400 metres. This is done to optimise model performance in the equatorial zone without unduly increasing computational costs. Upper ocean vertical mixing schemes are also generally more sophisticated than those used in standard global GCMs. For a review of ocean and coupled GCMs used to study ENSO dynamics, the reader is referred to Delecluse et al. (1998).

4.5.5 A Regional Model of the Southern Ocean

The Fine Resolution Antarctic Model (FRAM) is a primitive equation numerical model of the Southern Ocean between latitudes 24°S and 79°S. The model was initialised with $T = -2°\text{C}$ and $S = 36.69$ psu and relaxed to Levitus annual mean $T - S$ over 6 years. Surface wind forcing is that of Hellerman and Rosenstein (1983). Various strategies for gradual imposition of these fluxes is adopted to minimise numerical instability in the model spin-up phase (for details see de Cuevas, 1992, 1993). Model mixing schemes include a mixture of harmonic and biharmonic terms and a quadratic bottom friction stress. The total model run time is 16 years. The open boundary condition used in FRAM is a combination of a Sverdrup balance in the barotropic mode and a simple quasi-geostrophic balance and Orlanski radiation in the baroclinic terms (see Stevens, 1990, 1991 for further details).

In the final seasonal cycle phase of the model run, the Antarctic Circumpolar Current transport through Drake Passage oscillates between 195 and 200 Sv ($1\,\text{Sv} = 1 \times 10^6\ \text{m}^3\text{s}^{-1}$). This overly strong transport is a problem chronic to global-scale high resolution models. The main regions of eddy formation in the FRAM are in the Agulhas Current and along the path of the Circumpolar Current. The FRAM streamfunction simulated after the initial spin-up phase of the model run is illustrated in Fig. 4.16. Clearly apparent is the resolution of the ACC and its associated frontal dynamics and meanders. In addition, a substantial amount of eddy kinetic energy (figure not shown) is simulated in regions where the ACC encounters topographic features, such as the Campbell and Kerguelen Plateaus.

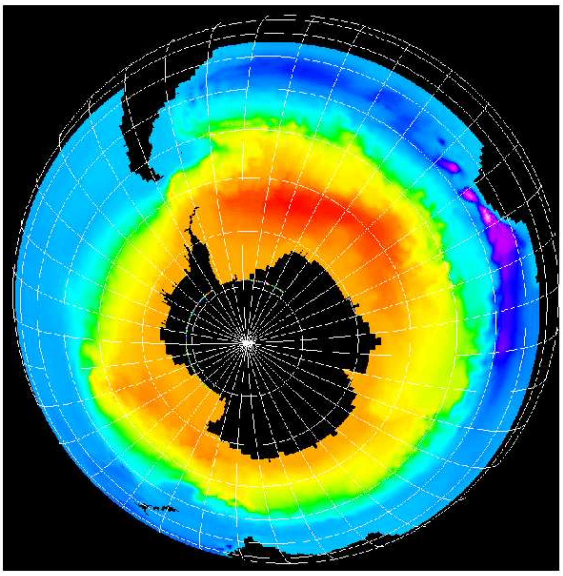

Fig. 4.16. Simulated barotropic streamfunction in the Fine Resolution Antarctic Model (FRAM) after the initial spin-up phase (from Webb et al., 1991).

4.5.6 A Coastal Ocean Model off Eastern Australia

An example of the POM configured for the EAC region is the NSW shelf model, which was developed at the UNSW Oceanography Laboratory (e.g., Gibbs et al., 1997; Oke and Middleton, 2001). The model utilises a curvilinear orthogonal grid with horizontal resolution of 5–20 km and extends along the entire coast of NSW. Observed surface and 250 m temperature fields are combined with Levitus climatology to produce the initial density field which is then used to determine the initial velocity field, via dynamic height calculations. With a constant inflow at the northern boundary and open boundary conditions which are relaxed to climatology at the east and south, the model has proved to be very useful for investigating the role that the EAC plays in nutrient enrichment of NSW coastal waters (e.g., Gibbs et al., 1997; Oke and Middleton, 2001). An example of the surface temperature and velocity fields modelled by the NSW shelf model for a period during January 1997 (from Oke and Middleton, 2001) is shown in Fig. 4.17. The modelled fields, which were qualitatively similar to observed temperature fields at the sea-surface and at a depth of 250 m, indicate that over a period of about a week, the EAC intensified over the continental shelf and extended southwards along the coast to the south of Sydney. A localised upwelling occurred immediately to the south of Port Stephens (indicated by the cold water mass near the coast). Through an analysis of the model fields it was hypothesised that the acceleration of the EAC over the narrow continental shelf near Smoky Cape resulted in uplifting of colder water which ultimately reached the surface in the vicinity of Port Stephens. The January 1997 period corresponded to a time when an algal bloom formed off Port Stephens. As a result of the modelling study it was suggested that topographically induced EAC-driven upwelling plays an important role in the nutrient enrichment of New South Wales coastal waters.

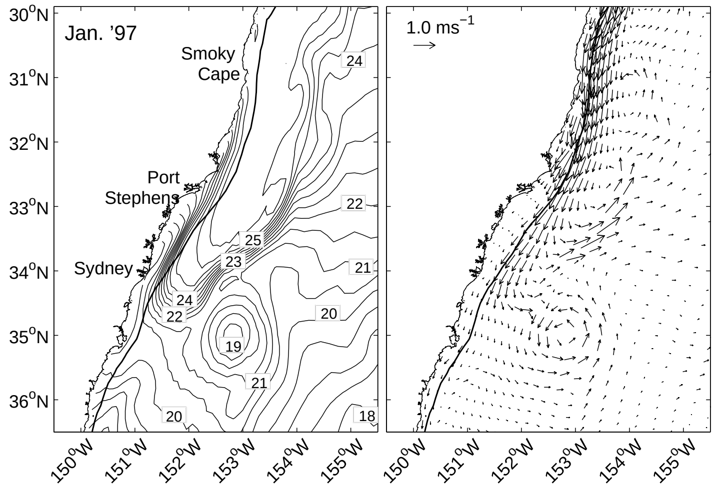

Fig. 4.17. Simulated surface temperature (left) and velocity (right) from the NSW shelf model, a configuration of the POM, showing fields for January 1997 (Oke and Middleton, 2001).

4.5.7 A Coastal Model of a River Plume

An example of a version of the POM utilised for a process-oriented study of the response of a river plume during upwelling favourable winds (Fong and Geyer, 2001) is outlined below. The model is configured for the northern hemisphere (f=10^{-4} s^{-1}) with a rectangular basin and idealized moderately steep nearshore bathymetry, that is typical of many narrow continental shelves. Freshwater is discharged via a short river/estuary system at the coast in the upper left hand corner of the 95 km × 450 km domain (Fig. 4.18). In the region of interest the resolution is less than 1 metre in the vertical, 1.5–3 km in the cross-shore direction and 3–6 km in the alongshore direction. A modified Mellor-Yamada turbulence sub-model is utilized (Mellor and Yamada, 1982; NunuzVaz and Simpson, 1994) and a recursive Smolarkiewicz advection scheme (Smolarkiewicz and Grabowski, 1990) is used to advect salt and temperature. A steady inflow of $0.1\,\mathrm{m\,s^{-1}}$ is imposed at the northern boundary to model the ambient continental shelf currents and a combination of clamped and radiative boundary conditions are employed at the offshore and southern boundaries. The salinity was initially 32 psu throughout the domain and the river plume is simulated by discharging freshwater (0 psu) from a point source at the coast at a constant rate of $1500\,\mathrm{m^3 s^{-1}}$. The plume is established in the absence of wind over a 1 month period (Fig. 4.18a), after which time constant 0.1 Pa upwelling favourable winds are applied over a 3-day period. The simulations demonstrate that, in response to upwelling favourable winds, the surface-trapped river plume widens and thins, and is advected offshore by the cross-shore Ekman transport (Fig. 4.18b–d). The thinned plume is susceptible to significant mixing due to the vertically sheared horizontal currents. Fong and Geyer (2001) utilise this configuration to investigate how the advective processes change the shape of the plume and how these advective motions alter the mixing of the plume with the ambient coastal waters.

4.6 Exploiting Ocean Observations

4.6.1 Model Assessment

The assessment of ocean models involves the comparison of a set of model variables or diagnostics with observations. Model assessment techniques range from simple qualitative comparisons through to statistical significance tests. It is convenient to look at large-scale and coastal models separately, as different quantities and time-scales are involved in such assessments.

Large-scale models. For large-scale models – those of an ocean basin-scale or greater – much model assessment is focused on long-term climatological hydrographic properties, particularly $T - S$, as well as integrated transport quantities like the net flow in the ACC. This is particularly the case for coarse resolution models, such as those incorporated into climate simulations. In such non-eddy-resolving models, ocean current speeds are slow and have none of the high-frequency variability associated with eddies or tides in the real ocean. Thus, direct comparison with observed current meter records is inappropriate. Instead, integrated transport measures, both in the horizontal and meridional plane, provide a more meaningful assessment of the model.

Water-mass formation is also most often assessed indirectly in coarse models; that is, by analysing model and observed $T - S$ rather than the model

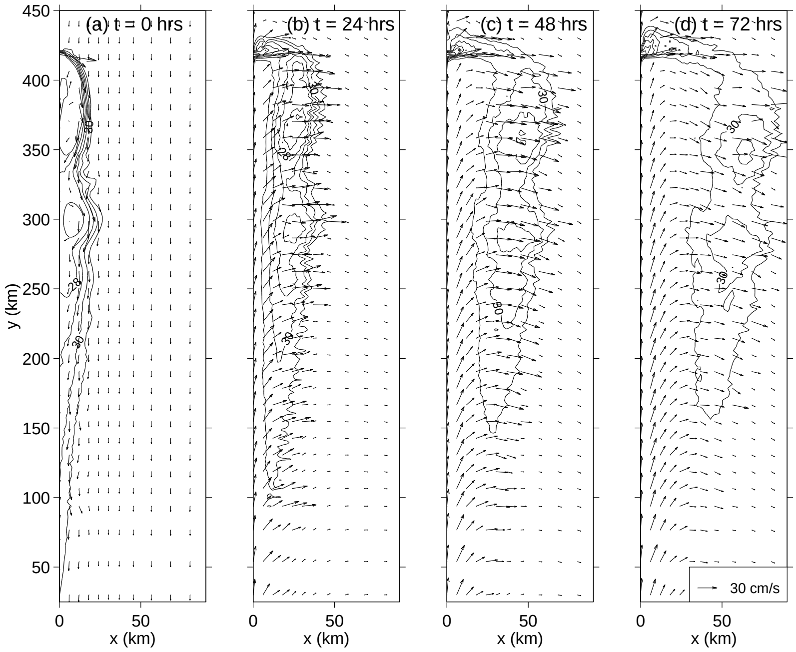

Fig. 4.18. Surface velocity and salinity for the evolution of a river plume during upwelling favourable wind conditions. (**a**) after 1 month of buoyancy forcing with no wind; (**b**)–(**d**) after 24, 48 and 72 hours of 0.1 Pa upwelling favourable winds. The scale for velocity is shown in panel (d) and the contour intervals are 1 psu for salinity (adapted from Fong and Geyer, 2001).

subduction/convection processes. This is partly because the processes that are linked with water-mass formation, such as convection, mixing, and deep currents, are extremely difficult to measure directly. In addition, such processes are subgrid-scale to a coarse resolution model, so assessment of them is best achieved by analysing their parameterised effects on model $T-S$ (e.g., England, 1993; Hirst and Cai, 1994; Hirst and McDougall, 1996).

Because temperature and salinity are prognostic variables in global ocean models and intrinsic in any definition of a water-mass, it is tempting to rely solely on them in the assessment of model water-mass formation. However, they provide only limited information on model water-mass formation rates, such as indicating the depth of rapid ventilation associated with surface mixing. Geochemical tracers, on the other hand, provide detailed information on the pathways and rates of water-mass renewal beneath the surface mixed layer, and therefore provide a stringent test of model behaviour. The main tracers that have been used in this context include tritium (Sarmiento, 1983), chlorofluorocarbons (England et al., 1994; England, 1995), and natural and bomb-produced radiocarbon (Toggweiler et al., 1989).

Assessment of large-scale eddy-resolving ocean models relies on quite different data sets to those discussed above. These models capture some degree of high-frequency variability, such as meanders in boundary currents as well as mesoscale eddy activity. They are also only run over interannual to decadal time-scales, so they do not simulate the long-term climatological water-mass properties of the ocean interior. A more stringent test of model behaviour in this situation is to compare properties such as the global eddy kinetic energy density or meridional fluxes of heat/freshwater. Figure 4.19 shows a comparison of the surface-height variability observed by satellite with that simulated in a 1/6° model (Maltrud et al., 1998). The model and observed eddy kinetic energy are in overall agreement, with high eddy activity where the ACC interacts with topography and in western boundary currents.

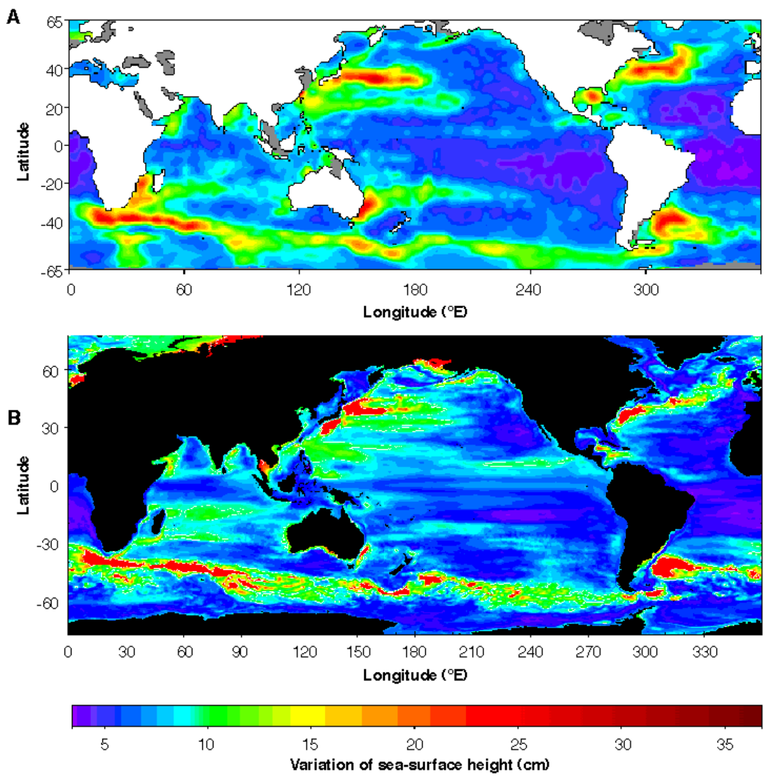

Fig. 4.19. Comparison between the surface-height variability (**a**) observed (Wunsch, 1996) with that (**b**) simulated in a 1/6° model (that of Maltrud et al., 1998) (from IPCC, 1995).

Regional and coastal ocean models. Many observational studies focus on continental shelves and coastal regions since this is where most recreational and commercial marine activities are focussed. Such studies typically involve spatially and temporally intense measurements of specific oceanic regions. As a result the validation of regional coastal ocean models is feasible for periods when observations are available. Typical observations of the coastal ocean for any given experiment include *in situ* measurements of currents and $T - S$ from an array of moored instruments at fixed locations or from shipboard surveys. Additionally, remotely sensed sea surface temperatures are often available. Together these data provide an incomplete picture of the coastal circulation which can be compared and contrasted with output from ocean models in order to either validate the model, or gain insight into the dominant dynamical processes that determine the circulation of the particular region. An example of a cross-section of temperature, salinity and potential density off Newport, Oregon observed during the OSU NOPP summer field season of 1999 is shown in Fig. 4.20 (Austin and Barth, 2001).

These sections show the isohals and isopycnals outcropping near the coast and a subsurface temperature maximum (e.g., the $9°$ isotherm) being subducted under the shallow surface mixed layer. The mechanism by which this subsurface temperature maximum is formed is unclear. Model analysis needs to be undertaken to determine the dynamical balances operating in the region.

Model validations usually involve a comparison between point source measurements and model output either qualitatively, by identifying similarities and differences in modelled and observed features, or quantitatively through statistical comparisons in the time domain (e.g., means, variances, correlations, empirical orthogonal functions and so on) or in the frequency domain (e.g., coherence, phase, gain). For a given application the validation requirements may be different. For example, if the timing and magnitude of temperature fluctuations are of interest in order to detect upwelling, then prediction of the mean temperature may be less important than the prediction of the variance, and it would be important for the model to be well correlated with observations. However, if coupling with the atmosphere is a concern, then the magnitude of the surface heat flux will depend on the mean surface temperature compared to the atmospheric temperature through the formulation of the sensible heat flux defined in (4.19).

A relatively recently developed method for observing the coastal ocean environment is the use of land-based high frequency (HF) Coastal Ocean Dynamics Application Radar (CODAR) arrays (e.g., Paduan and Rosenfield, 1996). CODAR measurements provide maps of near-surface ocean currents with high spatial ($\approx 1\,\text{km}$) and temporal ($\approx 10\,\text{minutes}$) resolution. The availability of these measurements provides modellers with an ideal opportunity to test the validity of their models. An example of a model-data comparison between an idealised configuration of the POM with CODAR data on the

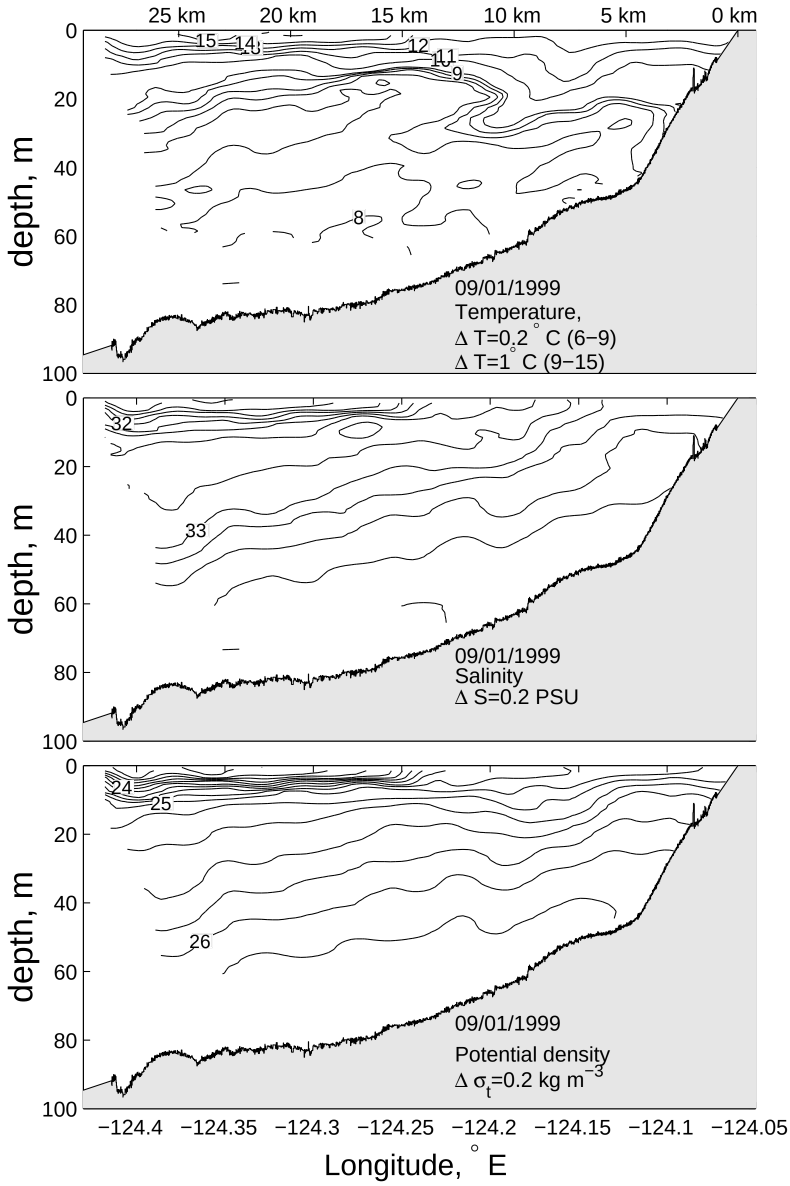

Fig. 4.20. Cross-shelf section of temperature (top), salinity (middle) and potential density (bottom) off Newport, Oregon observed during the OSU NOPP summer field season of 1999 (Austin and Barth, 2001).

Oregon continental shelf for the summer of 1998 is shown in Fig. 4.21 (from Oke et al., 2001). This figure shows a comparison between the modelled and observed mean surface currents (A and B), which indicates that the mean model fields are similar in structure and magnitude to the observed means. A comparison is also shown between the dominant spatial modes, obtained from an empirical orthogonal function (EOF) analysis of the modelled and observed fields (C–F). The spatial modes of an EOF analysis represent the structures of the variance fields. The percentage of the variance represented by each mode is shown in each panel indicating that 73% of the modelled variance and 48% of the observed variance is represented by these two EOFs. The first mode represents the acceleration of the coastal jet in response to upwelling favourable winds. The second mode represents the flow associated with upwelling relaxation (Gan and Allen, 2001), where a northward countercurrent is generated in response to the alongshore pressure gradients induced by the wind. Although the details of the modelled and observed means and the EOF modes differ, it is clear that the model is capturing a substantial amount of the true variability of the ocean in this region.

4.6.2 Inverse Methods and Data Assimilation

Data assimilation refers to the methods by which the inverse problem of the ocean circulation can be addressed. The inverse problem for the ocean circulation is the problem of inferring the state of the ocean circulation through a quantitative combination of theory and observations (Wunsch, 1996). Consider the system of equations that approximately and incompletely describes the ocean:

$$D\phi/dt = F + f \tag{4.23}$$

with

$$\begin{aligned}
&\text{Initial Conditions:} && \phi_i = I + i, \\
&\text{Boundary Conditions:} && \phi_b = B + b, \\
&\text{Observations:} && \phi_m^o = D_m + d_m
\end{aligned}$$

where ϕ represents the model state space, which consists of every model variable (e.g., u, v, w, T, S) at every model grid location; F, I, B and D represent the model forcing, initial conditions, boundary conditions and observations respectively; and f, i, b and d represent the errors in the model forecast, initial conditions, boundary conditions and observations respectively (Bennett, 1992). The inverse problem is to combine this information to obtain the most accurate and complete depiction of the ocean circulation that we can, given the resources available.

The forecast error f may be due to the approximations made by discretising the governing equations, or due to missing physics, if for example

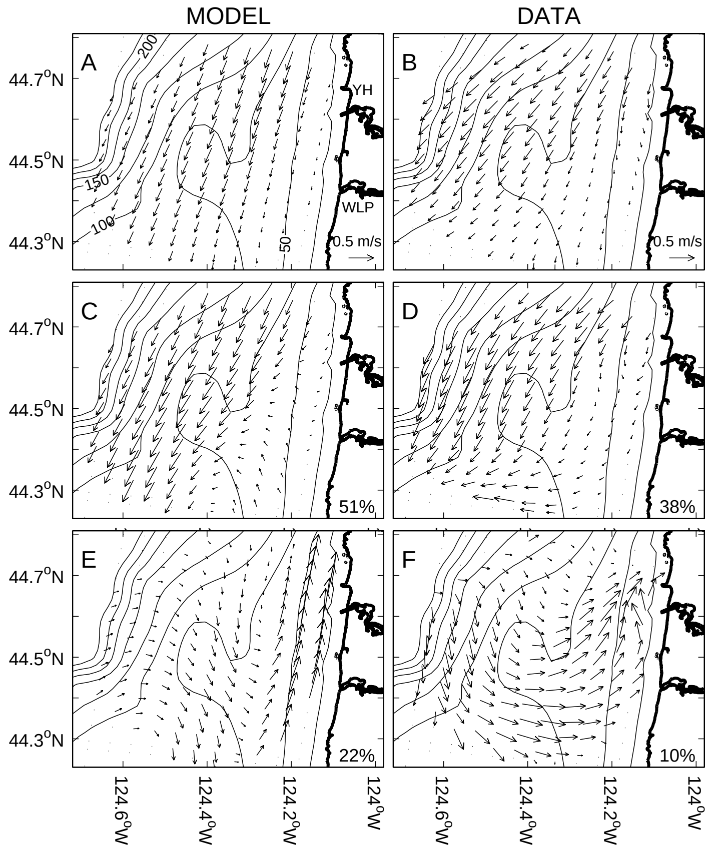

Fig. 4.21. Modelled (left) and observed (right) fields of surface currents off Oregon during the summer of 1998 showing the means (A–B) and the dominant spatial modes (C–F) calculated from an EOF analysis (Oke et al., 2001).

the non-linear terms in the equations are neglected. The error in the initial conditions i is a consequence of the fact that we can not know the precise state of the ocean at any moment in time. A model's initial condition will typically be derived from climatological data, or from an interpolation from sparse observations. The error in boundary conditions b may be due to the uncertainties in the applied wind or heat flux forcing; or in the case of regional models, due to the uncertainty in the lateral boundary conditions as well.

Finally, the observation error d_m represents the system noise which is the result of instrument error, measurement error and uncertainties in the observability of a particular oceanic variable. In order to produce the best possible depiction of the ocean circulation the method of least-squares is employed, where one attempts to find the solution to the governing equations, given the initial conditions, boundary conditions and observations, that is within the given error bounds of each component.

The simplest method for solving this inverse problem involve the application of sequential methods, namely optimal interpolation (e.g., Cohn et al., 1998) or the Kalman Filter (e.g., Miller, 1986). These methods attempt to optimally combine the observations and the dynamics to produce an analysis of the ocean ϕ^{a}. The analysis is produced by combining the model's forecast ϕ^{f} and the observations d_m using the so-called analysis equations:

$$\phi^{\mathrm{a}} = \phi^{\mathrm{f}} + \mathbf{K}(d_m - \mathbf{H}\phi^{\mathrm{f}}) \tag{4.24}$$

with

$$\mathbf{K} = \mathbf{P}^{\mathrm{f}}\mathbf{H}^{\mathrm{T}}(\mathbf{H}\mathbf{P}^{\mathrm{f}}\mathbf{H}^{\mathrm{T}} + \mathbf{R})$$

where $\mathbf{K}$ is the Gain matrix and $\mathbf{H}$ is an interpolation matrix that interpolates the model state onto the space of observations. The Gain matrix depends on the forecast error covariance matrix $\mathbf{P}^{\mathrm{f}}$ and the observation error covariance matrix $\mathbf{R}$. For sequential methods f, i and b are considered together and labelled the forecast error ϵ^{f}. The forecast and observation error covariances are given by

$$\mathbf{P}^{\mathrm{f}} = \langle \epsilon^{\mathrm{f}} \epsilon^{\mathrm{f}\,\mathrm{T}} \rangle$$

and

$$\mathbf{R} = \langle \epsilon^{\mathrm{o}} \epsilon^{\mathrm{o}\,\mathrm{T}} \rangle$$

respectively, where $\langle\cdot\rangle$ denotes a time average and ϵ^o is the observation error. For sequential methods an analysis of the model state is produced at each assimilation cycle which will depend on the time scales of the problem that is under investigation. In addition to the analysis equations presented above, the Kalman Filter also solves an equation for the time evolution of $\mathbf{P}^{\mathrm{f}}$. The implementation of the analysis equations involves the estimation of the forecast and observation error covariance matrices. In practise both ϵ^f and ϵ^o, and hence their covariances are unknown. The estimation of these covariance matrices involves assumptions about decorrelation length and time scales, and often about the homogeneity and isotropy of the model error fields. These matrices must be estimated prior to assimilation and their validity tested through a series of objective statistical tests after each assimilation (Bennett, 1992).

As an alternative to sequential methods, the generalized inverse method (e.g., Bennett et al., 1993; Errico, 1997) may be used. This approach involves the formulation of a quadratic penalty functional or cost function $\mathcal{J}$:

$$\mathcal{J} = W_f \int\int f^2 \mathrm{d}t\mathrm{d}x + W_i \int i^2 \mathrm{d}x + W_b \int b^2 \mathrm{d}t + W_d \sum {d_m}^2 \tag{4.25}$$

where W_f, W_i, W_b and W_d are positive weight functions for each component of the system described above. These weights are related to the above-mentioned forecast and observation error covariances and must also be chosen prior to assimilation. The cost function $\mathcal{J}$ is a single number for each depiction of ϕ. The cost function must be minimized by identifying the smallest values for f, i, b and d_m in the weighted least-squares sense. Once the global minimum of $\mathcal{J}$ is obtained, the optimal solution to ϕ is obtained. For a detailed discussion of the generalized inverse method and other methods for data assimilation the interested reader is referred to Bennett (1992) or Wunsch (1996).

The development and implementation of practical data assimilation techniques is vital if operational forecasting of the ocean circulation is going to become a reality. The development and maturity of remote sensing and *in situ* observing systems, the advances in scientific knowledge of the global and regional ocean circulation, and the development of sophisticated ocean models has made real-time observing and forecasting systems feasible. As outlined above data assimilation enables available observations derived either remotely, from satellites or radar systems, or *in situ*, from moored instruments, drifters or shipboard surveys, to be combined with ocean models in order to produce a complete depiction of the ocean circulation at time scales of a few days and space scales of several tens of kilometres. The Global Ocean Data Assimilation Experiment (GODAE) is an experiment that is designed to demonstrate the practicality and feasibility of routine, real-time global ocean data assimilation and prediction (Smith and Lefebvre, 1998).

All weather forecasting systems that are presently in operation utilise data assimilation in some form, through either initialisation to an objective map of the atmospheric state or through more sophistocated assimilation techniques. Forecasting the ocean circulation presents all of the same difficulties and challenges as weather forecasting, except that ocean observations are much more sparse compared to observations of the atmosphere. Consequently the development of reliable and practical data assimilation systems for ocean forecasting is more crucial since we must endeavor to take full advantage of the limited observations that are available.

4.6.3 Applications of Data Assimilation to Coastal Ocean Models

One application of sub-optimal sequential data assimilation to a regional, primitive equation model of the Oregon continental shelf circulation is outlined below. This application involved assimilation of surface velocity data obtained from a land-based HF CODAR array during the summer of 1998 (Oke et al., 2000). The surface information was projected over the entire water column in order to correct velocities and density at depth. In order to demonstrate how well the surface information was projected over depth the depth-averaged velocity, in 80 m of water, obtained from a moored acoustic doppler profiler (ADP) is compared with the model hindcast with and without assimilation (Fig. 4.22). The magnitude of the complex correlation between the observations and the model without assimilation is 0.42, and with assimilation is 0.76, indicating that the assimilation improved the hindcast by approximately 50%, demonstrating its potential for coastal ocean modeling.

4.6.4 Application of Data Assimilation to Large-scale Models

An example of a project that is endeavouring to develop a forecast system for the global oceans is the GODAE. This development is a very challenging task, both from a scientific and technical perspective. Issues that must be overcome include development of advanced models; development of efficient and effective assimilation schemes; estimation of error statistics; data management and quality control; and access to large computer facilities and communication systems. The main benefits of a global nowcast and forecast system include the availability of reliable initial conditions for coupled ocean-atmosphere models which are used for climate and seasonal forecasting; reliable boundary conditions for high resolution regional ocean models; as well as applications to marine safety, fisheries, offshore industry and management of continental shelf and coastal areas.

4.6.5 Variational Data Assimilation, Example

Table 4.1. Comparison of various solutions for the M_2 and K_1 surface elevation in the Barents Sea: RMS errors (cm) (from Kurapov and Kivman, 1999).

Model	Resolution & Domain	M_2 RMS error (cm)	K_1 RMS error (cm)
Gjevik et al. (1994)	25×25 km	7.4	2.6
Non-linear, no assimilation	Barents Sea		
Kowalik and Proshutinsky (1995)	14×14 km	6.9	1.6
Non-linear, no assimilation	Arctic Ocean		
Kivman (1997)	$1^\circ \times 1^\circ$	5.0	2.2
GIM, finite difference	Arctic Ocean		
Kurapov and Kivman (1999)	1–52 km	3.6	1.2
GIM, finite element.	Barents Sea		

The generalised inverse of a high-resolution finite element model of the Barents Sea, which is a part of the Arctic Ocean, based on the linearised shallow water equations was developed by Kurapov and Kivman (1999).

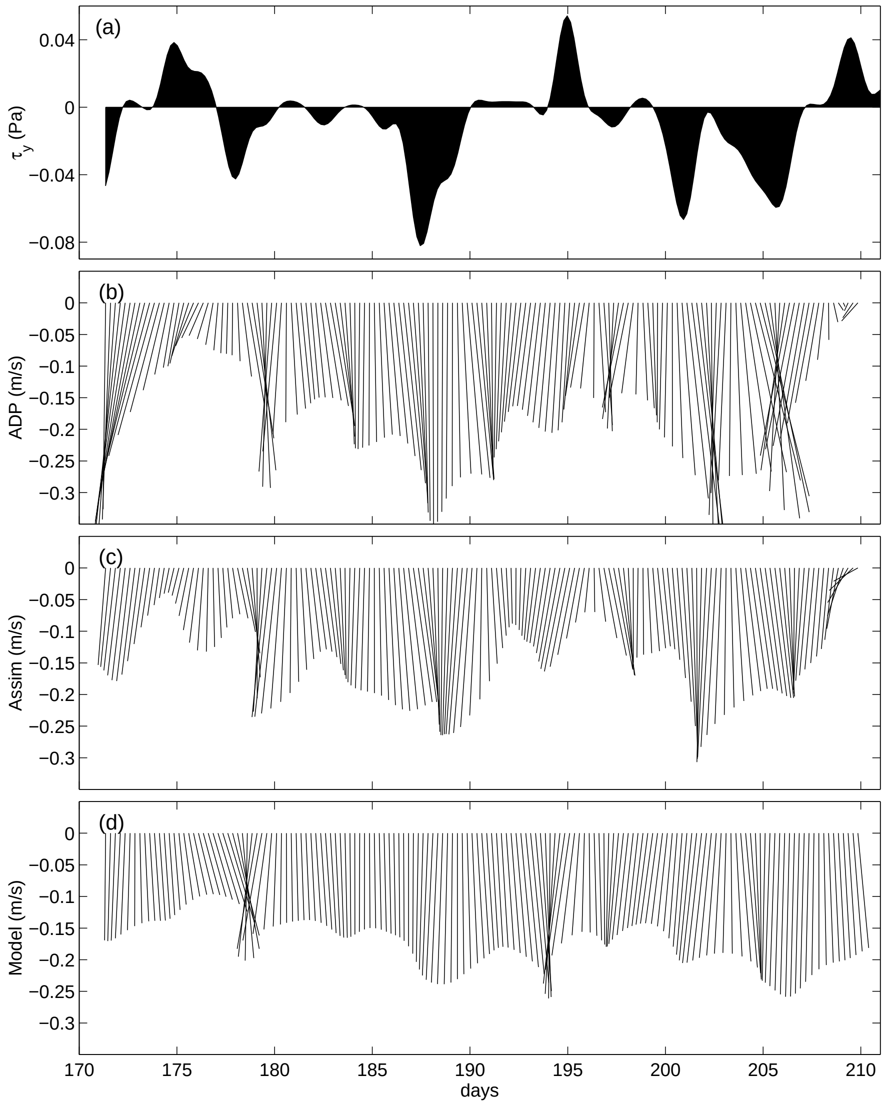

Fig. 4.22. (**a**) Alongshore wind stress from Newport, Oregon 1998; vector stick plots of depth-averaged velocities from (**b**) a moored ADP v^o(at 80 m depth), (**c**) model simulation with assimilation of surface velocity data v^a, and (**d**) model simulation with no assimilation v^m. Correlations: $C(v^o, v^m) = 0.42$; $C(v^o, v^a) = 0.76$ (from Oke et al., 2001).

This inverse model involved assimilation of tidal constituents from 47 coastal tide gauges. The resulting assimilation was validated by a comparison of the analysed tidal elevations with independent tide gauges in the interior of the domain and near the open boundaries. The results indicate that with a low weight given to the open boundary conditions in the cost function, the generalised inverse is capable of reproducing tidal elevations of the dominant tidal constituents with greater precision than other more complicated models with larger domains that did not utilise data assimilation. These comparisons are summarised in Table 4.1. While the linear model clearly has significant errors due to the neglected physics, particularly in the shallow waters, these comparisons demonstrate that its generalised inverse provides a very effective, dynamically based, interpolator for this region. This example demonstrates the power of inverse methods for ocean modeling, particularly for hindcasting and nowcasting.

4.7 Concluding Remarks

Ocean circulation models form an important component of oceanographic and climate research. Applications range from simulations of flow in bays and harbours through to coastal, regional, and global-scale models. In this chapter we reviewed the governing equations, model grid systems, boundary conditions, and the parameterisation of subgrid-scale processes. We also gave specific examples of a number of models, from large-scale climate related simulations, to coastal experiments, river plume models and tidal flows. The use of observational data was also reviewed, from model assessment to data assimilation and inverse model techniques. The future directions of ocean modelling research are farreaching; they include refinements of subgrid-scale parameterisations, use of higher resolution models, development of improved numerical schemes, applications of data assimilation towards predictive systems, and coupled modelling with climate and biological modules.